Journal of Natural Fibers

ISSN: 1544-0478 (Print) 1544-046X (Online) Journal homepage: www.tandfonline.com/journals/wjnf20

Sustainable Renewable Biofuel Production Toward Pyrolysis of Fibers Biowaste *Agave Americana L.* and Thermodynamics Mechanisms Kinetic Parameters Triplet Assessment

Imen Lalaymia, Ahmed Belaadi, Hassan Alshahrani, Djamel Ghernaout & Herbert Mukalazi

To cite this article: Imen Lalaymia, Ahmed Belaadi, Hassan Alshahrani, Djamel Ghernaout & Herbert Mukalazi (2025) Sustainable Renewable Biofuel Production Toward Pyrolysis of Fibers Biowaste *Agave Americana L.* and Thermodynamics Mechanisms Kinetic Parameters Triplet Assessment, Journal of Natural Fibers, 22:1, 2537069, DOI: 10.1080/15440478.2025.2537069

To link to this article: https://doi.org/10.1080/15440478.2025.2537069

JOURNAL OF NATURAL FIBERS
2025, VOL. 22, NO. 1, 2537069
https://doi.org/10.1080/15440478.2025.2537069

Sustainable Renewable Biofuel Production Toward Pyrolysis of Fibers Biowaste *Agave Americana L.* and Thermodynamics Mechanisms Kinetic Parameters Triplet Assessment

Imen Lalaymia[a], Ahmed Belaadi[a], Hassan Alshahrani[b], Djamel Ghernaout[c,d], and Herbert Mukalazi[e]

[a]Department of Mechanical Engineering, Faculty of Technology, University 20 August 1955- Skikda, Skikda, Algeria; [b]Department of Mechanical Engineering, College of Engineering, Najran University, Najran, Saudi Arabia; [c]Chemical Engineering Department, College of Engineering, University of Ha'il, Ha'il, Saudi Arabia; [d]Chemical Engineering Department, Faculty of Engineering, University of Blida, Blida, Algeria; [e]Department of Mathematics and Statistics, Kyambogo University, Kampala, Uganda

ABSTRACT

This study explores the thermal degradation behavior and pyrolysis kinetics of fibers derived from the flower stalk of Agave americana waste (FSSAW), aiming to assess their suitability for bioenergy applications. Non-isothermal thermogravimetric analysis (TGA) was conducted at heating rates of 30, 40, and 50 °C/min. Kinetic modeling using the Coats – Redfern method evaluated 36 solid-state reaction models to determine the activation energy-Ea and pre-exponential factor (lnA). The highest Ea was observed for Model M22, increasing from 218.87 kJ/mol at 30 °C/min to 252.73 kJ/mol at 50 °C/min, while the lowest Ea, 4.22 kJ/mol, was recorded for Model M19. These results indicate the presence of both complex and simple reaction mechanisms, with a general increase in Ea at higher heating rates, consistent with the kinetic compensation effect. Thermodynamic analysis revealed a maximum enthalpy change (ΔH) of 249.65 kJ/mol, a maximum Gibbs free energy change (ΔG) of 390.81 kJ/mol, and a minimum entropy change (ΔS) of −0.31 kJ/mol·K, confirming that the pyrolysis process is endothermic and non-spontaneous, leading to a more ordered transition state. Criado's master plot technique further validated Model M16 (random nucleation and growth) as the most representative mechanism during early decomposition stages. However, deviations at higher conversions suggest the occurrence of multi-step processes, including diffusion and char formation.

摘要

本研究探讨了龙舌兰废弃物（FSSAW）花茎纤维的热降解行为和热解动力学，旨在评估其在生物能源应用中的适用性. 在30、40和50的加热速率下进行非等温热重分析（TGA）°C/分钟. 使用Coats-Redfern方法的动力学建模评估了36个固态反应模型，以确定活化能Ea和指数前因子（lnA）. M22型的Ea最高，从218.87上升 30时的kJ/mol °C/min至252.73 50时的kJ/mol °C/min，最低Ea为4.22 记录了M19型的kJ/mol. 这些结果表明，存在复杂和简单的反应机制，在较高的加热速率下Ea普遍增加，这与动力学补偿效应一致. 热力学分析显示，最大焓变（ΔH）为249.65 kJ/mol，最大吉布斯自由能变化（ΔG）为390.81 kJ/mol，最小熵变（ΔS）为-0.31 kJ/mol·K，证实热解过程是吸热和非自发的，导致更有序的过渡态. Criado的主图技术进一步验证了M16模型（随机成核和生长）是早期分解阶段最具代表性的机制. 然而，较高转化率的偏差表明发生了多步骤过程，包括扩散和炭形成.

KEYWORDS

Pyrolysis; Kinetics; Coats-redfern method; thermodynamic analysis; criado master plot; Waste

关键词

热解; 热解; Coats-Redfern法; 热力学分析; 克里多主情节; 浪费

Introduction and literature review

In response to the substantial increase in energy demand, considerable efforts have been dedicated to the development of renewable energy sources and alternative fuels, leading to notable advancements. Among these, lignocellulosic biomass has attracted growing attention as a renewable energy resource, particularly for applications such as pyrolysis, combustion, and other energy conversion processes (Ding et al. 2019). Biomass energy is widely acknowledged in the near future as the renewable resource most likely to promote sustainable development (Van De Velden et al. 2010). Currently, biomass accounts for 14% of global major source of energy, yet much of it is wasted because of inefficient utilization and unsustainable practices.

CONTACT Herbert Mukalazi hmukalazi@kyu.ac.ug Department of Mathematics and Statistics, Kyambogo University, Kampala, Uganda
Supplemental data for this article can be accessed online at https://doi.org/10.1080/15440478.2025.2537069

Unlocking its full potential requires the adoption of innovative approaches and advanced technologies (Li et al. 2017). It is commonly known that waste-to-energy technologies like pyrolysis, gasification, and combustion are efficient ways to turn leftover biomass into biofuels and bioenergy (Vieira et al. 2016). Pyrolysis has recently received more attention because to its ease of use, low operating costs, high inherent safety, and reduced emissions of pollutants as compared to gasification and combustion (Navarro et al. 2018). As non-native raw materials, invasive grasses, exhibit large yields even on barren and marginal lands (Salama 2020), making them readily available at low cost. Moreover, their substantial carbon content offers promising potential for bioenergy production. Among the various technological pathways for the profitable conversion of lignocellulosic biomass, thermochemical processes including the well-established methods of pyrolysis, combustion, and gasification are particularly noteworthy Pyrolysis offers several advantages over combustion and gasification, including moderate costs, operational simplicity, and lower emissions of polluting gases (Constantino et al. 2019).

The fiber of Agave americana (*FSSAW*), cultivated notably in arid and semi-arid areas such as Ain Achir in Annaba, Algeria, represents a promising renewable and sustainable biomass resource (Lalaymia, Belaadi, and Ghernaout 2025). Utilizing FSSA fibers for bioenergy production can help decrease dependence on nonrenewable fossil fuels and reduce environmental pollution (Lalaymia, Belaadi, et al. 2024). This aligns with the growing need for renewable, sustainable, and eco-friendly materials, driven by the intensive use of fossil fuels and the environmental issues they cause (Lalaymia, Bedjaoui, et al. 2024). Among the available conversion methods, combustion stands out as a well-established and effective thermal process for treating solid biomass, enabling the production of valuable biofuels such as volatiles, charcoal, and bio-oil (Lalaymia et al. 2023).

Various kinetic methods are frequently applied to investigate the thermal degradation behavior of biomass materials. The Coats-Redfern method, a model-fitting approach, is often used to determine activation energy and identify the most probable reaction mechanism by fitting experimental data to different kinetic models (Ferfari et al. 2024). In contrast, the Flynn-Wall-Ozawa (FWO) and the Kissinger-Akahira-Sunose (KAS) techniques don't rely on models. The isoconversional techniques that allow for activation energy is calculated without assuming a particular reaction model (Dubdub and Al-Yaari 2020). These methods analyze the variation of decomposition temperatures under different heating rates, offering a more detailed understanding of the kinetic behavior across the entire conversion range (Stamopoulos, Tserpes, and Dentsoras 2018). The thermal and kinetic information necessary for applying these methods is typically obtained through Thermogravimetric Analysis (TGA), a powerful tool that measures the mass loss of a substance under regulated air circumstances as a function of temperature or time. TGA offers important information on the thermal stability and breakdown properties of biomass (Y. Wang et al. 2024b).

Many researchers have investigated the deterioration caused by heat characteristics of various biomass materials, including the evaluation of kinetic parameters under both inert and oxidative atmospheres. In general, thermal analysis results indicate that the predominant activation energy factor influencing the reactivity during biomass thermal degradation (Inayat, Jamil, Forruque, et al. 2023). Elmay el al (Elmay et al. 2016). was assessed while inert (nitrogen) and oxidative (air) atmospheres by using thermogravimetric analysis (TGA). The kinetic parameters were determined through isoconversional techniques, such as Kissinger – Akahira – Sunose (KAS) and Flynn – Wall – Ozawa (FWO), to evaluate how activation energy changes with conversion degree. Furthermore, the Coats – Redfern method was applied to identify the most probable solid-state mechanisms describing the degradation process. The results provide crucial details regarding the pyrolysis and combustion characteristics of FSSA fibers, contributing to their valorization in bioenergy applications. Naqvi et al. (2015) examined the behavior of thermal degradation. of paddy husk under both non-catalytic and catalytic conditions. They used thermogravimetric analysis (TGA) to monitor the mass loss of the biomass as it was heated, providing insights into its thermal stability and decomposition patterns. To interpret the TGA data, the Coats – Redfern method – a widely used integral method for kinetic analysis was employed to determine the pre-exponential variables and activation energy related to the pyrolysis processes. The study identified two distinct temperature regions during the pyrolysis process: 240–330°C is Region I, and 360–450°C is Region II. It was discovered that adding zeolite catalysts (ZSM-5, MCM-22, and ITQ-2) decreased the activation energy in Region I, indicating an enhanced decomposition rate. Conversely,

in Region II, the presence of catalysts increased the activation energy, suggesting a different reaction mechanism or a change in the rate-limiting step. The authors concluded that both chemical reaction and diffusion-controlled mechanisms could effectively describe the pyrolysis behavior of paddy husk, emphasizing the complexity of biomass thermal decomposition and the influence of catalytic additives (Zuo et al. 2017). explored the pyrolysis characteristics of three types of biomass in the presence of copper slag as a heat carrier. TGA experiments were conducted to analyze the thermal decomposition behavior. Kinetic parameters were determined using the Coats – Redfern method, revealing that the pyrolysis process conformed well to the shrinking core model (A3). The addition of copper slag was discovered to encourage both primary pyrolysis reactions and alkanes and alkenes breaking down, although it did not notablely reduce the activation energy. Using TGA data evaluated using the Coats – Redfern approach with 27 distinct model equations, Postawa et al. (2022) concentrated on figuring out the kinetic characteristics of maize biomass. Activation energies ranged from 6.5 to 71.6 kJ/mol, and the study found several reaction orders across several pyrolysis phases. The results demonstrated how complicated biomass pyrolysis is and how using a variety of kinetic models is essential to properly characterizing the process. Dewayanto, Isha, and Ridzuan (2014) used TGA to investigate the catalytic pyrolysis of decanter cake, a by-product of milling palm oil. The kinetic behavior was examined using the Coats – Redfern method, which revealed two primary stages of breakdown. While the second stage adhered to a second-order kinetic model, the first stage followed a first-order one. In all phases, it was discovered that the presence of catalysts decreased the activation energy; the lowest activation energy was recorded at a 10 weight percent catalyst loading. Dhaundiyal et al. (2018)used TGA to examine *Parthenium hysterophorus's* heat deterioration. Kinetic parameters were determined using the Coats – Redfern method and model-free techniques like Kissinger – Akahira – Sunose (KAS) and Flynn – Wall – Ozawa (FWO). Dehydration, active pyrolysis, and passive pyrolysis were the three primary phases of the decomposition process. Despite the Coats – Redfern model's shortcomings at varying heating rates, the study concluded that diffusion models offered a satisfactory fit for the experimental results.

It is imperative to look at untreated waste materials because there aren't many empirical studies on the pyrolysis behavior of *FSAAW* fiber. In this situation, a more thorough comprehension of the pyrolysis reaction mechanisms requires taking into account the impact of changing the heating rate (β). Examining kinetic characteristics under various β values enhances the accuracy of activation energy (Ea) computations and fortifies the dependability of reaction mechanism models.

Analyses focus point

A thorough comparison between our findings and previously reported data is provided to reinforce the validity of our analysis. The consequences of the different heating rates are the main focus of this investigation (β) on the stability and efficiency of volatile chemical release during pyrolysis. Using the Coats – Redfern method (CRM), precise kinetic and thermodynamic parameters are determined to predict reaction mechanisms and support the optimization of large-scale conversion systems. Overall, the key focus of this work is on the thermal degradation and kinetic analysis of lignocellulosic materials, aiming to achieve a comprehensive understanding of their pyrolysis behavior under different β conditions. A thorough comparison between our findings and the data from the literature is given in Table 1.

Novelty of the current work

The current work is new since it thoroughly examines fibers from *FSSAW*, an undiscovered biomass feedstock for the generation of bioenergy. Activation energy (Ea), enthalpy change (ΔH), Gibbs free energy change (ΔG), and entropy change (ΔS) are among the important kinetic and thermodynamic parameters that are determined in this study's first analysis of the pyrolysis behavior of *FSSAW* fibers using sophisticated techniques like Thermogravimetric Analysis (TGA). The application of multiple isoconversional methods, including Friedman, Vyazovkin, and Coats-Redfern, allows for an in-depth understanding of the pyrolysis kinetics, offering robust and reliable results. Additionally, the use of Criado's master plot technique introduces a novel approach to identifying the reaction mechanisms governing the thermal

Table 1. Comparison of kinetic parameters in this study and previous studies.

Specimen	β (°C/min)	Average activation energy E (kJ/mol)	Average pre-exponential factor A (1/min)	Reaction model g(α)	Reference
FSSAW	30,40,50	**68.78**	**19.61**	$[-\ln(1-\alpha)]^4$	This study
Banana fiber waste	20, 30, 40	145.25–182.10	3.12×10^{9} to 5.67×10^{10}	$[1-(1-\alpha)^{1/2}]^2$	(Yunus et al. 2013)
Coconut shell powder	10, 20, 30	195.40	2.41×10^{13}	$(1-\alpha)^{-1/3}-1$	(Sun and Cheng 2002)
Rice straw pellets	5, 15, 25, 35	121.73–138.90	7.26×10^{8} to 2.11×10^{9}	$[-\ln(1-\alpha)]^3$	(X. Wang and Ni 2017)
Corn cob biochar	10, 20, 30, 40	210.85–245.55	5.15×10^{12} to 7.89×10^{13}	$1-(1-\alpha)^{2/3}$	(Felipe et al. 2017)
Waste coffee grounds	15, 25, 35	162.40–175.90	8.20×10^{11} to 1.02×10^{12}	[(1 - α)^-1/ 2–1]^2	(Ballesteros, Teixeira, and Mussatto 2014)
Palm kernel shells	10, 20, 30	202.10	1.73×10^{14}	$[1/(1-\alpha)]-1$	(Saddawi, Jones, and Williams 2012)
Sunflower husk	10, 20, 30	155.35	2.97×10^{11}	$1-(1-\alpha)^{1/3}$	(Lemoine et al. 2013)

degradation of *FSSAW* fibers. Overall, this work contributes valuable thermodynamic insights that can enhance the development of bioenergy systems according to natural fiber feedstocks, positioning *FSSAW* fibers as a promising source for renewable energy applications.

Materials and methods

Materials

Agave americana produces yellow flowers (Lalaymia et al. 2023). Once the plant flowers, it dies, leaving behind a sturdy stalk that is typically discarded but holds notable value for natural fiber (NF) production. The process begins by peeling the *FSAAW* and cutting them into 50 cm segments. These segments are then soaked in water for 30–45 days at 30°C to 45°C. Anaerobic bacterial activity speeds up the fiber extraction process during soaking. The fibers are hand sorted, cleaned, and allowed to air dry after soaking. This method not only makes effective use of Agave americana's otherwise waste stalks but also provides a sustainable source of natural fibers, supporting the development of eco-friendly materials (Lalaymia, Bedjaoui, et al. 2024).

Characterization of FSSAW

Fourier Transform Infrared Spectroscopy (FTIR), along with proximate and ultimate analyses, were employed to characterize the FSSAW biomass (Apaydın Varol and Mutlu 2023). Detailed descriptions of the proximate, ultimate, and compositional analyses are provided elsewhere. The functional groups present in the FSSAW fiber samples were examined using FTIR spectroscopy. Spectra were recorded at a resolution of 1 cm^{-1} over a scan range of 4000–400 cm^{-1} to identify the chemical bonds and functional groups in the material (Ni et al. 2021).

Physicochemical analysis for FSSAW

The physicochemical composition of *FSSAW* was determined through proximate and ultimate analyses. In accordance with the GB/T 212–2008 standard, proximate analysis was carried out using a muffle furnace to determine the amounts of ash, fixed carbon, and volatile matter (Inayat, Jamil, Ahmed, et al. 2023). Ultimate analysis was carried out with a CHNS/O elemental analyzer (Batna, Algeria) to measure carbon, hydrogen, nitrogen, and oxygen contents (V et al. 1989). Together, these analyses provide a complete characterization of the elemental composition and thermal properties of *FSSAW*.

Thermogravimetric analyses

Thermogravimetric analysis (TGA) of FSSAW fibers was conducted using a METTLER TOLEDO TGA/ DSC 3+ instrument, equipped with a high-precision balance and automatic baseline correction features

(Shagali et al. 2023). The fibers, weighing approximately 10 ± 0.2 mg, were placed in alumina crucibles and heated from room temperature to 800°C under a constant nitrogen flow of 60 mL/min to ensure an inert atmosphere. The experiments were performed at five distinct heating rates (5, 10, 20, 30, and 50 °C/min) to investigate the kinetic behavior (Anca-Couce et al. 2020).

Equipment calibration

The instrument was calibrated before each set of experiments using certified reference materials (Indium and Zinc) for temperature calibration, and standard calibration weights for mass accuracy, in accordance with ISO 11,358–1:2014 standards. The temperature accuracy was ± 1°C, while the mass accuracy was within ±0.01 mg. Drift in the baseline was corrected using blank runs under the same conditions.

Measurement uncertainty

Each TGA test was repeated three times, and results were averaged to reduce random error. The relative standard deviation (RSD) for the mass loss and temperature at peak degradation remained below 2.5%, ensuring good reproducibility. Small fluctuations in mass loss (±1%) were observed due to inherent sample heterogeneity and surface moisture variability.

Kinetic study for FSAAW fibers

The kinetic analysis accounts for varying heating rates β, which influence the apparent activation energy and reaction rates due to thermal lag and heat transfer effects. Multiple heating rates improve the reliability of the kinetic parameters A kinetic analysis of *FSAAW* fiber pyrolysis was carried out using Arrhenius's law (Ali, Tariq, Raza, et al. 2021). The reaction rate is described by:

$$\frac{d\alpha}{dt} = k(T)f(\alpha) \tag{1}$$

In this equation, the conversion fraction, α, is defined as:

$$\alpha = \frac{m_0 - m_i}{m_0 - m_f} \tag{2}$$

Here, m_0 is the initial mass of the sample, m_i; is its mass at any given point during pyrolysis, and mf represents the final, residual mass.

According to the Arrhenius equation, the temperature-dependent rate constant, k(T), is:

$$k(T) = A\exp\left(-\frac{E_a}{RT}\right) \tag{3}$$

where T is the absolute temperature in Kelvin, The pre-exponential factor, A, represents the frequency of collisions in min^{-1}, E_a is the activation energy in kJ/mol, and R is the universal gas constant (0.008314 $kJ{\cdot}mol^{-1}{\cdot}K^{-1}$) (Sharma, Joshi, and Singh, n.d.).

At a constant heating rate, $\beta = \frac{dT}{dt}$, combining the previous equations yields:

$$\frac{d\alpha}{dT} = \frac{A}{\beta}\exp\left(-\frac{E_a}{RT}\right)f(\alpha) \tag{4}$$

The reaction model's integral form can be found using:

$$g(\alpha) = \int_0^{\alpha}\frac{d\alpha}{f(\alpha)}$$

$$g(\alpha) = \frac{A}{\beta}\int_{T_0}^{T}\left(-\frac{E_a}{RT}\right)dT \tag{5}$$

Since this integral lacks an analytical answer and uses a variety of approximations models are employed to evaluate the kinetic parameters for *FSAAW* fibers effectively (Bourmaud and Baley 2010).

Model fit

One essential element among the kinetic triplets is the kinetic model, f(α). This function can be determined through model-fit techniques, such as Criado's method of master plots and the CR approach, which are effective tools for analyzing the mechanism and dynamics of pyrolytic decomposition.

Coats – Redfern Approach

The Coats – Redfern method was selected not only to estimate activation energy but also to assess and compare 36 solid-state reaction models for identifying the most suitable decomposition mechanism of FSSAW fibers. Unlike model-free methods such as FWO and KAS, which provide average Ea values, the CR method enables direct model fitting and facilitates mechanistic interpretation. Its use yielded high correlation coefficients ($R^2 > 0.94$), and the derived kinetic parameters supported the calculation of thermodynamic properties (ΔH, ΔG, ΔS). Although model-free methods are more precise for Ea, the CR method was intentionally used here for its strength in reaction mechanism identification (Ali, Tariq, Naqvi, et al. 2021). The Coats-Redfern integral assumes Ea/RT⟩1, allowing simplification of the temperature integral to a linear form, which enables straightforward linear regression for kinetic parameter extraction. This approximation holds true in the temperature ranges studied. The CR model's fundamental equation is provided by:

$$\ln\left[\frac{g(\alpha)}{T^2}\right] = ln\frac{AR}{\beta E_a}\left(1-\frac{2RT}{E_a}\right) - \frac{E_a}{RT} \tag{6}$$

The equivalent integral form of the kinetic model to different reaction processes is represented by g (α) in this equation, as described in Table 2. By plotting $\ln\left[\frac{g(\alpha)}{T^2}\right]$ against 1/T, a linear relationship is obtained. The intercept of this line can be used to determine the pre-exponential factor (A), while the slope provides a measure of the activation energy (E_a) (Inayat, Jamil, Ahmed, et al. 2023). Although the specific form of g (α) may differ depending on the reaction mechanism, most solid-state reactions are categorized into one of the 36 groups listed in Table 2.

Criado's master plot method

A straightforward model-fitting technique for determining the reaction mechanism controlling the pyrolysis kinetics is Criado's master plot method (V et al. 1989). The method is based on the following equation:

$$\frac{Z(\alpha)}{Z(0.5)} = \frac{f(\alpha)\times g(\alpha)}{f(0.5)\times g(0.5)} = \left(\frac{T_\alpha}{T_{0.5}}\right)^2 \frac{\left(\frac{d\alpha}{dt}\right)_\alpha}{\left(\frac{d\alpha}{dt}\right)_{0.5}} \tag{7}$$

Here, the temperature and conversion rate for α = 0.5 are denoted as T 0.5 and (dα/dt)0.5. The equation's left-hand side represents theoretical reduced curves for various reaction processes, expressed as f (α)g(α)/f (0.5) g (0.5) The right-hand side, derived from the experimental data, includes the temperature and conversion rate at any α. By comparing experimental data to these theoretical curves, the most suitable reaction mechanism can be determined. The assumed reaction model determines the particular shape of f (α), as described in Table 2.

The kinetic analysis of FSAAW fiber pyrolysis relies on the Arrhenius law combined with solid-state reaction models to describe the temperature-dependent conversion behavior. The Coats-Redfern method linearizes the integral form of the rate equation by approximating the temperature integral, enabling the extraction of the activation energy (Ea) and pre-exponential factor (A) through linear regression of $\ln[\frac{g(\alpha)}{T^2}]$ versus 1/T. This approach assumes a specific reaction model f(α) characterizing the decomposition mechanism, which is crucial for mechanistic interpretation. Complementarily, Criado's master plot method

Table 2. The common reaction model/mechanism of solid-state pyrolysis.

Model No.	$g(\alpha)$	$f(\alpha)$	Rate-determining reaction mechanism
(1) **Chemical process or mechanism non-invoking equations**			
M-1	$1-(1-\alpha)^{2/3}$	$3/2(1-\alpha)^{1/3}$	Chemical reaction
M-2	$1-(1-\alpha)^{1/4}$	$4(1-\alpha)^{3/4}$	Chemical reaction
M3	$(1-\alpha)^{-1/2}-1$	$2(1-\alpha)^{3/2}$	Chemical reaction
M-4	$(1-\alpha)^{-1}-1$	$(1-\alpha)^{2}$	Chemical reaction
M-5	$(1-\alpha)^{-2}-1$	$1/2(1-\alpha)^{3}$	Chemical reaction
M-6	$(1-\alpha)^{-3}-1$	$1/3(1-\alpha)^{4}$	Chemical reaction
M-7	$1-(1-\alpha)^{2}$	$1/2(1-\alpha)$	Chemical reaction
M-8	$1-(1-\alpha)^{3}$	$1/3(1-\alpha)^{2}$	Chemical reaction
M-9	$1-(1-\alpha)^{4}$	$1/4(1-\alpha)^{3}$	Chemical reaction
(2) **Acceleratory rate equations**			
M-10	$\alpha^{3/2}$	$2/3\alpha^{-1/2}$	Nucleation
M-11	$\alpha^{1/2}$	$2\alpha^{1/2}$	Nucleation
M-12	$\alpha^{1/3}$	$3\alpha^{2/3}$	Nucleation
M-13	$\alpha^{1/4}$	$4\alpha^{3/4}$	Nucleation
M-14	$\ln\alpha$	α	Nucleation
(3) **Sigmoidal rate equations or random nucleation and subsequent growth**			
M-15	$-\ln(1-\alpha)$	$1-\alpha$	Assumed random nucleation and its subsequent growth
M-16	$[-\ln(1-\alpha)]^{2/3}$	$3/2(1-\alpha)[-\ln(1-\alpha)]^{1/3}$	Assumed random nucleation and its subsequent growth
M-17	$[-\ln(1-\alpha)]^{1/2}$	$2(1-\alpha)[-\ln(1-\alpha)]^{1/2}$	Assumed random nucleation and its subsequent growth
M-18	$[-\ln(1-\alpha)]^{1/3}$	$3(1-\alpha)[-\ln(1-\alpha)]^{2/3}$	Assumed random nucleation and its subsequent growth
M-19	$[-\ln(1-\alpha)]^{1/4}$	$4(1-\alpha)[-\ln(1-\alpha)]^{3/4}$	Assumed random nucleation and its subsequent growth
M-20	$[-\ln(1-\alpha)]^{2}$	$1/2(1-\alpha)[-\ln(1-\alpha)]^{-1}$	Assumed random nucleation and its subsequent growth
M-21	$[-\ln(1-\alpha)]^{3}$	$1/3(1-\alpha)[-\ln(1-\alpha)]^{-2}$	Assumed random nucleation and its subsequent growth
M-22	$[-\ln(1-\alpha)]^{4}$	$1/4(1-\alpha)[-\ln(1-\alpha)]^{-3}$	Assumed random nucleation and its subsequent growth
M-23	$\ln\alpha/(1-\alpha)$	$\alpha/(1-\alpha)$	Branching nuclei
(4) **Deceleratory rate equations**			
(4.1) **Phase boundary reaction**			
M-24	?	1	Contracting disk
M-25	$1-(1-\alpha)^{1/2}$	$2(1-\alpha)^{1/2}$	Contracting cylinder (cylindrical symmetry)
M-26	$1-(1-\alpha)^{1/3}$	$3(1-\alpha)^{2/3}$	Contracting sphere (spherical symmetry)
(4.2) **Based on the diffusion mechanism**			
M-27	α^{2}	$1/2\alpha$	One-dimensional diffusion
M-28	$\left[1-(1-\alpha)^{1/2}\right]^{1/2}$	$4\left\{(1-\alpha)[1-(1-\alpha)]^{1/2}\right\}^{1/2}$	Two-dimensional diffusion
M-29	$\alpha+(1-\alpha)\ln(1-\alpha)$	$[-\ln(1-\alpha)]^{-1}$	Two-dimensional diffusion
M-30	$\left[1-(1-\alpha)^{1/3}\right]^{2}$	$(3/2)(1-\alpha)^{2/3}\left[1-(1-\alpha)^{1/3}\right]^{-1}$	Three-dimensional diffusion. spherical symmetry
M-31	$1-2/3\alpha-(1-\alpha)^{2/3}$	$(3/2)\left[(1-\alpha)^{-1/3}-1\right]^{-1}$	Three-dimensional diffusion. cylindrical symmetry
M-32	$\left[(1-\alpha)^{-1/3}-1\right]^{2}$	$(3/2)(1-\alpha)^{4/3}\left[(1-\alpha)^{-1/3}-1\right]^{-1}$	Three-dimensional diffusion
M-33	$\left[(1+\alpha)^{1/3}-1\right]^{2}$	$(3/2)(1+\alpha)^{2/3}\left[(1+\alpha)^{1/3}-1\right]^{-1}$	Three-dimensional diffusion
M-34	$1+2/3\alpha-(1+\alpha)^{2/3}$	$(3/2)\left[(1+\alpha)^{-1/3}-1\right]^{-1}$	Three-dimensional diffusion
M-35	$\left[(1+\alpha)^{-1/3}-1\right]^{2}$	$(3/2)(1+\alpha)^{4/3}\left[(1+\alpha)^{-1/3}-1\right]^{-1}$	Three-dimensional diffusion
M-36	$\left[1-(1-\alpha)^{1/3}\right]^{1/2}$	$6(1-\alpha)^{2/3}\left[1-(1-\alpha)^{1/3}\right]^{1/2}$	Three-dimensional diffusion

offers a model-fitting graphical tool by comparing normalized experimental data to theoretical curves, allowing the qualitative identification of the controlling reaction mechanism without direct calculation of kinetic parameters. Together, these mathematically justified methods provide a comprehensive framework for deciphering the complex, multi-step pyrolysis kinetics of lignocellulosic fibers like FSAAW.

Thermodynamic analysis

Thermodynamic analysis involves evaluating key physical quantities such as Gibbs free energy (ΔG), entropy (ΔS), and enthalpy (ΔH), which reflect the system's disorder, internal energy, and thermodynamic potential, respectively (Torres-Sciancalepore et al. 2022). These properties are closely linked to kinetic parameters and serve as important indicators of the material's thermal stability (Gayathri

et al. 2020). The nature of the reaction, whether it is endothermic or exothermic, is determined by the enthalpy change between the reactants and products under specific conditions (M. Raza et al. 2022). It is crucial to compute thermodynamic parameters like ΔH, ΔG, and ΔS in order to evaluate the viability of the thermal degradation process (Estrada, Linero, and Ramírez 2013). The equations used for these calculations are presented in references (Goumghar et al. 2022; Ma et al. 2023; Y. Wang et al. 2024a).

$$A^* = \frac{x.E.\exp\left(\frac{E}{R.T_P}\right)}{R.T_P^2} \tag{8}$$

$$\Delta H = E - RT \tag{9}$$

$$\Delta G = E + R.R.T_P.\ln\left(\frac{K_B T_P}{h.A}\right) \tag{10}$$

$$\Delta S = \frac{\Delta H - \Delta G}{T_P} \tag{11}$$

- h represents Planck's constant, valued at 6.626×10^{-34} J·s,
- K_B is Boltzmann's constant, equal to 1.381×10^{-23} J·K^{-1},
- T_p denotes the peak temperature (in Kelvin) obtained from the DTG (Derivative Thermogravimetric) curve.

Results and discussion

FSSAW FT-IR analysis

The distinctive absorption bands corresponding to the main chemical components, including cellulose, hemicelluloses, and lignin, were identified by analyzing the FTIR spectra of the *FSAAW* fibers, which are shown in Figure 1. It is the O – H stretching vibrations that are responsible for the broad absorption band seen at about 3342 cm^{-1} (Huang et al. 2020), which show that there exist hydrogen bonds in cellulose. The C – H stretching vibrations of the methyl and methylene groups (CH and CH_2) are shown by the peak at 2904 cm^{-1} (Zsinka 2024), demonstrating that both cellulose and hemicelluloses are present. C = O stretching vibrations are linked to an absorption band at 1731 cm^{-1}, which usually corresponds to ester groups present in hemicelluloses. The aromatic C = C stretching of lignin's phenylpropanoid units is responsible for the peak at 1591 cm^{-1}, confirming the substance's aromatic nature. At 1377 cm^{-1}, a noticeable peak is ascribed to C – H bending effects (Xu et al. 2018), commonly observed in polysaccharide structures. Additionally, the peak at 1243 cm^{-1} corresponds to C – O stretching vibrations from the acetyl groups present in lignin. Dual peaks around 1034 cm^{-1} are linked to C – O and O – H vibrations (Komandur, Vinu, and Mohanty 2022), suggesting the co-presence of lignin and cellulose. Finally, an absorption band near 597 cm^{-1} is associated with out-of-plane bending vibrations of C – OH groups (Gupta, Thengane, and Mahajani 2020), further supporting the presence of phenolic structures in the lignin. These spectral observations are consistent with previous studies (refer to Table 3) and confirm the complex chemical structure of *FSAAW* fibers, characterized by multiple functional groups.

Physicochemical properties of FSSAW

Table 4 summarizes the physicochemical characterization of FSAAW fibers. The moisture content of 6.24% and a high volatile matter content of 76.85% indicate strong potential for pyrolytic conversion. The low ash content (2.31%) and fixed carbon (14.60%) further affirm its suitability as a bioenergy feedstock. Ultimate analysis reveals significant carbon (48.12%) and hydrogen (6.02%) contents, contributing to a relatively high higher heating value (HHV) of 19.25 MJ/kg. The substantial cellulose (49.87%) and lignin (28.53%)

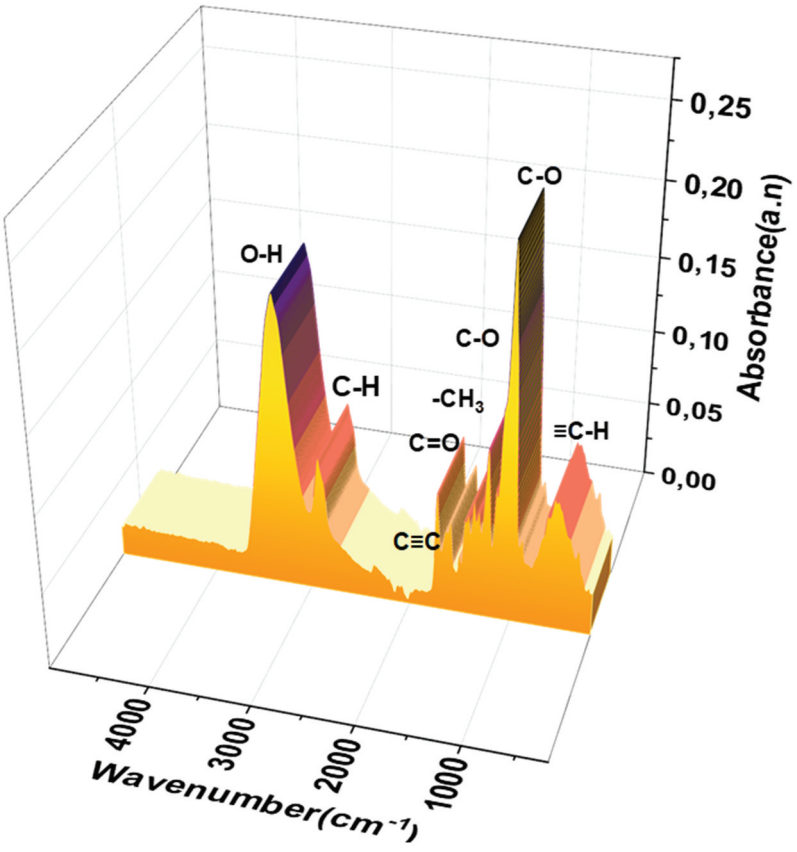

Figure 1. The FT-IR spectrum was taken for the *FSSAW* fibers used in this study.

Table 3. The functional groups detected in the *Agave americana biowaste*.

Wavenumbers (cm^{-1})	Band position (cm^{-1})	Functional group
3200–3600	3332	Alcohol
2850–3000	2899	Alkane
2100–2260	2299	Alkyne
1795–1850	1724	Acid
1580–1615	1498	Aromatic
1350–1480	1391	Alkane
1180–1260	1220	Phenolic
1020–1120	1022	Ether
600–700	582	Alkyne

Table 4. Physicochemical analysis of *FSSAW*.

Physicochemical analysis	Properties	Values
Proximate analysis (wt. %)	Moisture content	6.24
	Volatile matter	76.85
	Ash content	2.31
	Fixed carbon	14.60
Ultimate analysis (wt. %)	C	48.12
	H	6.02
	O	44.25
	N	0.90
	S	0.29
Compositional analysis (wt. %)	Cellulose	49.87
	Hemicellulose	18.14
	Lignin	28.53
	H/C	1.50
	O/C	0.69
	HHV (MJ/kg)	19.25
	Molecular Formula	$CH_{1.50}O_{0.69}N_{0.010}S_{0.00259}$

fractions favor the production of bio-oil and biochar during thermal decomposition. Collectively, these properties suggest FSAAW fibers are excellent candidates for sustainable thermal conversion processes.

Thermal degradation

Figure 2 shows the TG and DTG characteristics of *FSAAW* fibers (M. Raza et al. 2022). The thermal degradation proceeds in multiple stages corresponding to moisture loss, hemicellulose, cellulose, and lignin decomposition. Moisture evaporation occurs below ~ 120°C, preparing the biomass for pyrolysis. Hemicellulose decomposes rapidly between 150°C and 300°C, releasing volatiles and causing substantial mass loss (Gerald Arul Selvan et al. 2023), Cellulose degradation follows between 300°C and 400°C, leading to significant volatile emission and char formation. The lignin phase degrades gradually from 400°C to 800°C, producing solid char and gaseous byproducts such as CO_2 and CO (Parida, Pradhan, and Pandit 2023). Higher heating rates (40–50 °C/min) induce thermal lag, shifting decomposition peaks to elevated temperatures and broadening the DTG curves due to insufficient reaction time, as seen in Figure 2. Conversely, at moderate heating rates (e.g., 30 °C/min), decomposition stages are more distinctly separated (Parida, Pradhan, and Pandit 2023). Unlike hemicellulose and cellulose, lignin's breakdown is more complex and slower, often involving multiple steps, and it leads to the formation of solid char residue and the evolution of gases such as CO_2 and CO. The rate at which heat is applied plays a significant role in the thermal decomposition of *FSAAW* fiber. At higher heating rates (e.g., 40–50 °C/min), the decomposition peaks shift to higher temperatures due to thermal lag, meaning the reaction does not have enough time to proceed at lower temperatures. This results in broader, delayed thermal responses in the DTG profiles, with overlapping decomposition stages. Conversely, at moderate heating rates (e.g., 30 °C/min), the degradation stages are more distinct, with clearer separation between the peaks corresponding to moisture evaporation, hemicellulose breakdown, cellulose degradation, and lignin decomposition (Yu et al. 2020). Additionally, increased heating rates result in slightly higher char residues, consistent with the kinetic compensation effect where faster heating limits complete volatilization (Sarkar and Wang 2020). The thermal degradation behavior of *FSAAW* fibers is consistent with findings from other lignocellulosic biomass studies, including wheat straw, palm fronds, and rice husks. For instance, Hu et al. (2021) reported that Guanzhong wheat straw decomposes in three main stages: moisture evaporation below 150°C, hemicellulose degradation between 180°C and 260°C, and cellulose breakdown from 320°C to 380°C, followed by a broad lignin decomposition from 400°C to 800°C. These ranges are highly comparable to *FSAAW*, which shows hemicellulose degradation from 150°C to 300°C, cellulose from 300°C to 400°C, and lignin from 400°C to 800°C. Similarly, El, Tarek, and Mohamed (2024) analyzed the thermal behavior of various biomasses and found that increasing the heating rate led to a shift of DTG peaks to higher temperatures due to thermal laga phenomenon also observed in *FSAAW*, especially at 50 °C/min. Additionally, Li et al.

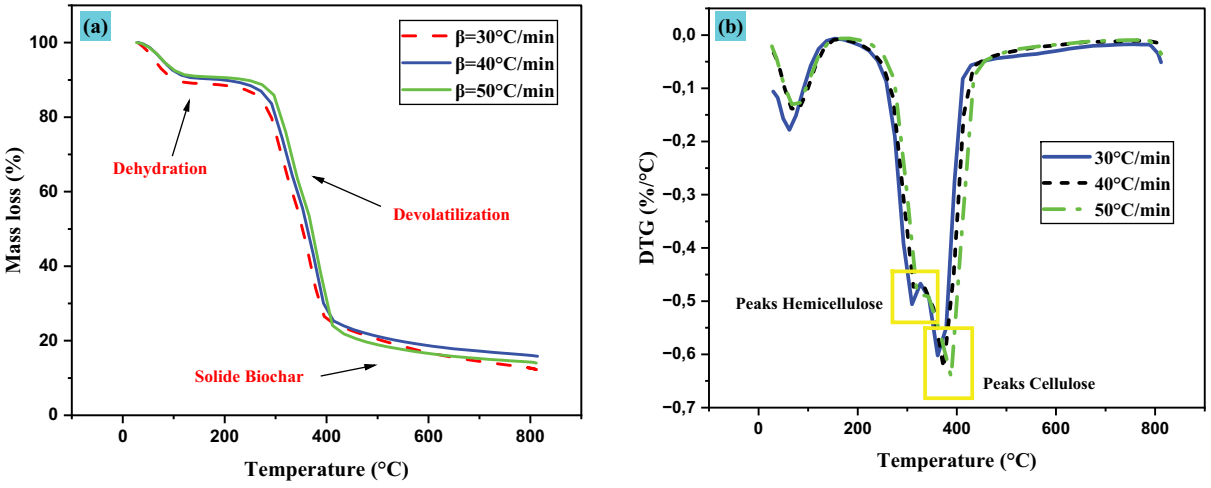

Figure 2. (a) TGA and (b) DTG curves of the three samples at different heating rates.

(Lei et al. 2023) emphasized that higher heating rates result in broader decomposition stages and increased char yield, findings that are mirrored in FSAAW results. In all three comparative studies, the DTG peak temperatures for cellulose ranged from 360°C to 370°C, closely matching the *FSAAW* peak at ~ 365°C. These consistent patterns in thermal degradation stages, heating rate effects, and char yield affirm the reliability of *FSAAW*'s pyrolytic profile and support its suitability as a promising feedstock for bioenergy applications. Overall, these findings highlight the intricate relationship between heating rate and thermal behavior in biomass fibers like *FSAAW*, underscoring the need for careful consideration of heating rates in kinetic and thermodynamic analyses.

Kinetic analysis

The thermogravimetric analysis (TGA) of *FSSAW* fiber reveals a typical three-stage thermal degradation pathway common to lignocellulosic materials. As shown in Figure (a), the first stage, occurring below approximately 120°C, involves moisture evaporation, resulting in a minor mass loss. This is followed by the primary pyrolytic decomposition phase, between roughly 200°C and 400°C, during which hemicellulose and cellulose undergo significant thermal degradation, leading to the release of volatile matter and the greatest weight reduction. The third and final stage, extending from 400°C to 800°C (Kumar et al. 2021), is attributed to the gradual and complex breakdown of lignin, culminating in the formation of a stable char residue. A comparison of decomposition profiles at heating rates of 10 °C/min and 20 °C/min shows that as the heating rate increases, the decomposition curves shift toward higher temperatures (Gurukarthik Babu et al. 2019). This thermal shift, caused by reduced reaction time and thermal lag, highlights the kinetic compensation effect. Additionally, a slightly greater char yield at 20 °C/min suggests that higher heating rates inhibit complete volatilization, favoring residue formation (Selvan et al. 2022).

Further insights into the thermal behavior are illustrated in Figure 3a,b, which presents the variations of the degree of conversion (α) and its derivative (dα/dT) as functions of temperature (T) at heating rates of 30, 40, and 50 °C/min. The figure shows a clear trend where, for a given α, the temperature T increases with heating rate β, indicating that the thermal breakdown process is delayed by greater heating rates. Interestingly, the influence of increasing T and β on dα/dT tends to balance out, although the temperature according to the highest value of dα/dT shifts progressively higher with increasing β. Table 5 provides a quantitative summary of these trends, showing the maximum dα/dT values, the average dα/dT for the whole pyrolysis range, as well as the temperatures at which these maxima occur. The Coats-Redfern (CR)

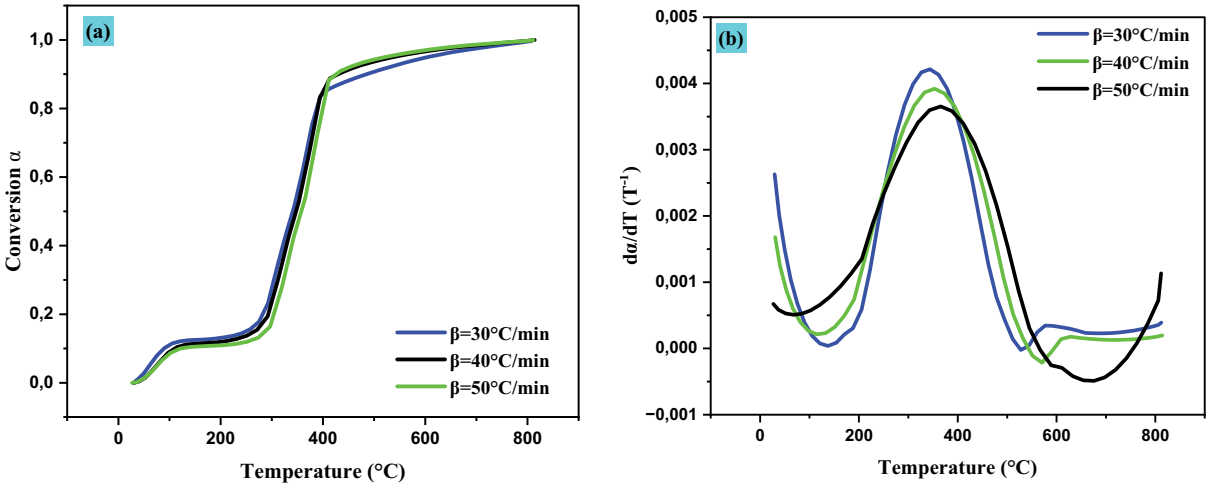

Figure 3. Variation of α and dα/dT with temperature (T).

Table 5. Maximum and average dα/dT, and corresponding T.

β (°C/min)	Maximum dα/dT(T^{-1})/T (°C)	Average dα/dT(T^{-1})
30	3.8×10^{-3}/340.50	1.15×10^{-3}
40	3.6×10^{-3}/350.30	1.10×10^{-3}
50	3.4×10^{-3}/360.20	1.05×10^{-3}

Table 6. Results calculation lnA and E of method CR based on data thermogravimetric at 30, 40, and 50 °C/min.

	30°C /min			40°C/min			50°C /min		
No	E(KJ/mol)	lnA	R^2	E(KJ/mol)	lnA	R^2	E(KJ/mol)	lnA	R^2
M-1	35.58	9.58	0.984	40.05	11.10	0.982	44.51	8.21	0.980
M-2	42.55	11.95	0.991	46.14	13.16	0.990	51.18	10.29	0.989
M-3	57.27	16.94	0.990	58.62	17.40	0.995	64.98	48.49	0.992
M-4	68.60	20.79	0.983	68.00	20.59	0.994	75.44	48.36	0.988
M-5	94.55	29.60	0.964	89.14	27.77	0.985	99.14	13.63	0.971
M-6	124.12	39.65	0.948	113.05	35.89	0.973	125.95	9.44	0.953
M-10	50.95	14.80	0.978	58.42	17.33	0.976	64.62	38.93	0.974
M-11	10.25	0.98	0.937	12.77	1.83	0.942	14.73	1.41	0.940
M-15	47.15	13.51	0.992	50.08	14.50	0.993	55.53	20.87	0.992
M-16	28.07	7.03	0.991	30.04	7.70	0.992	33.62	5.00	0.990
M-17	18.53	3.79	0.988	20.02	4.29	0.989	22.66	2.59	0.988
M-18	8.99	0.55	0.978	10.00	0.89	0.980	11.70	1.08	0.979
M-19	4.22	−1.06	0.943	4.98	−0.80	0.952	6.23	0.52	0.957
M-20	104.39	32.95	0.994	110.22	34.93	0.995	121.26	12.75	0.993
M-21	161.63	52.38	0.994	170.35	55.35	0.995	186.99	8.62	0.994
M-22	218.87	71.82	0.994	230.49	75.77	0.995	252.73	7.46	0.994
M-24	30.60	7.89	0.973	35.59	9.58	0.971	39.68	6.55	0.986
M-25	38.27	10.49	0.988	42.42	11.90	0.986	47.10	9.14	0.985
M-26	41.09	11.45	0.991	44.88	12.74	0.989	49.79	9.99	0.988
M-27	71.30	21.71	0.980	81.24	25.08	0.979	89.56	32.80	0.976
M-28	14.09	2.28	0.977	16.18	2.99	0.975	18.45	1.84	0.974
M-29	80.81	24.94	0.988	89.82	28.00	0.986	98.86	24.53	0.984
M-30	92.28	28.83	0.993	99.80	31.39	0.991	109.79	22.54	0.990
M-31	84.61	26.23	0.990	93.13	29.12	0.988	102.48	31.05	0.987
M-32	117.61	37.44	0.992	121.40	38.72	0.996	133.64	13.43	0.994
M-33	62.42	18.69	0.974	72.32	22.06	0.972	80.08	51.33	0.968
M-34	65.27	19.66	0.976	75.19	23.03	0.974	83.12	94.46	0.971
M-35	54.24	15.92	0.965	64.03	19.24	0.963	71.26	20.30	0.958
M-36	15.50	2.76	0.983	17.41	3.41	0.981	19.79	1.99	0.980

method was used to determine the activation energy (Ea) and pre-exponential factor (lnA) in order to better examine the dynamics of *FSSAW* fiber pyrolysis. Table 6 displays the obtained correlation coefficients (R^2), lnA, and Ea for a variety of reaction models at varying heating rates. This information is useful for modeling and refining thermal conversion processes employing *FSSAW* fibers. Table 6 lists the correlation coefficients (R^2), activation energy (Ea), and pre-exponential factor (lnA) derived from the Coats-Redfern (CR) approach for a range of reaction models (M1–M36) at three distinct heating rates: °C/min at 30, 40, and 50 (Alves et al. 2019). The kinetic parameters exhibit significant variation depending on the model and heating rate, reflecting the complexity of the pyrolytic decomposition of *FSSAW* fiber. Among the models, M22 consistently yields the highest activation energy across all heating rates, with Ea values rising from 218.87 kJ/mol at 30 °C/min to 252.73 kJ/mol at 50 °C/min, indicating a highly energy-demanding reaction pathway, similar findings were reported by C. Chen (2020), who used the Coats – Redfern approach to analyze Dunaliella salina pyrolysis and observed Ea values between 180 and 260 kJ/mol, depending on the additive used, indicating a comparable energy demand for decomposition under thermal conditions. In contrast, models such as M19 and M18 show very low Ea values (as low as 4.22 kJ/mol for M19 at 30 °C/min), suggesting these may represent early-stage or surface-limited reactions. A general trend of increasing activation energy with increasing heating rate is observed for most models, consistent with the kinetic compensation effect. This is also accompanied by variations in the lnA values, with several models (notably M22, M21, M6, and M30) showing exceptionally high pre-exponential factors, indicative of complex reaction mechanisms involving multiple steps or transition states showing in Figure 4. The correlation coefficients (R^2) remain above 0.94 for nearly all models, affirming the robustness of the CR method in fitting the experimental TGA data. However, models such as M15, M16, and M3 exhibit particularly high R^2 values (≥0.992), suggesting they provide the best fit for the pyrolytic kinetics of *FSSAW* fiber (Loy et al. 2018). The kinetic data also confirm that the choice of model has a significant impact on calculated parameters, emphasizing the importance of selecting appropriate reaction mechanisms for accurate interpretation of thermal degradation behavior, In addition, the application of Criado's master plot in the present work confirmed a sigmoidal reaction mechanism (M16), dominated by nucleation and growth, particularly in the $0.15 < \alpha < 0.55$ range. This agrees with the work of Agnihotri and Kumar (2024), who

used Criado's method to study soybean stalk pyrolysis and identified similar reaction pathways governed by progressive nucleation, highlighting the multistep nature of biomass degradation. These findings provide critical insight for optimizing pyrolysis conditions and reactor design for bioenergy applications involving *FSSAW* fiber. The integral method's fitting curves for determining the kinetic parameters of biomass pyrolysis based on various diffusion and reaction order models are displayed in Figure 5. The kinetic data reveal that all reaction mechanism models exhibit a consistent trend: the apparent activation energy (Ea) tends to increase as the heating rate (HR) rises from 30°C to 50°C/min. This observation highlights the influence of HR on pyrolysis kinetics. Notably, the pre-exponential factor (lnA) generally shows a decreasing tendency with increasing HR, suggesting a reduction in the frequency of molecular collisions or transition state formation at elevated heating rates. This inverse relationship higher Ea with lower lnA follows a typical kinetic compensation effect. The rise at a higher Ea HRs can be attributed to thermal lag and the reduced time for heat transfer, which delays the reaction onset and demands more energy for decomposition. Conversely, the drop in lnA implies that while it takes more energy. to initiate the reaction, the molecular events leading to the transition state become less frequent. Additionally, the correlation coefficient (R^2) serves as an indicator of model fidelity. In some cases, R^2 values decrease with increasing HR, indicating that certain models may not capture the kinetics accurately under faster heating conditions. These results highlight how crucial it is to choose the right models. and understanding thermal lag effects in kinetic studies of *FSSAW* fiber pyrolysis (Klinger et al. 2018).

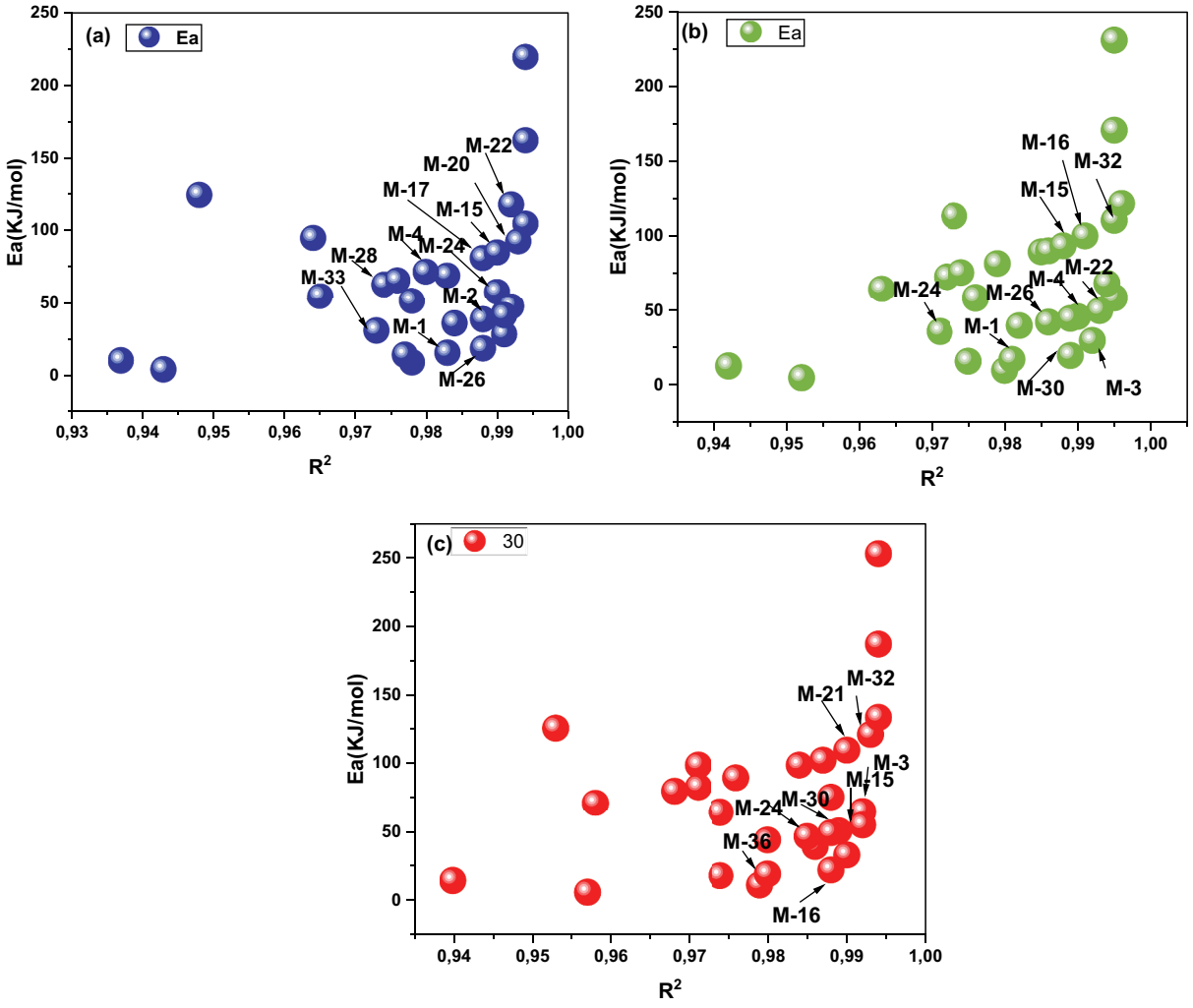

Figure 4. Relationship between correlation coefficient (R^2) and activation energy (Ea) at heating rates of (a) 30 °C/min, (b) 40 °C/min, and 50 °C/min.

Figure 6 illustrates the activation energy (Ea) profiles for the pyrolysis of *FSSAW* fiber at heating rates of 30°C, 40°C, and 50°C/min, as determined using the reaction mechanism (RM) model. The lowest energy barrier required to start the thermal breakdown of biomass and release volatile chemicals is known as the activation energy (Gourier et al. 2014, Klinger et al., 2018). In other words, Ea reflects the energy required to trigger the chemical reactions during pyrolysis. Noticeable variations were observed in the Ea profiles across different conversion levels, indicating the complex nature of *FSSAW* decomposition. Typically, reactions with higher Ea require higher temperatures and longer durations to complete thermal breakdown (Hameed et al. 2018). A notable rise in Ea was noted for all heating rates at a conversion threshold of $\alpha = 0.6$, while only slight changes were noted at lower conversions ($\alpha < 0.3$), highlighting the strong dependence of Ea on the extent of conversion. This variation suggests that the structural properties of *FSSAW* and the multistep nature of its thermal degradation influence the reaction pathway. A pronounced change in Ea with increasing conversion may reflect sequential or parallel reaction mechanisms, while a relatively stable Ea would indicate a simpler, single-step degradation process. The observed increase in Ea greater conversion rates could be linked to with secondary reactions such as char formation, crosslinking, and polycondensation, which require greater energy input. These findings emphasize the complexity of *FSSAW* fiber pyrolysis and the role of conversion-dependent kinetics in determining the thermal behavior of lignocellulosic materials (Sharifzadeh et al. 2019). Furthermore, the observed kinetic compensation effect, where increased heating rates raised Ea while lnA decreased was consistent with studies on high-ash sewage sludge pyrolysis by S. Raza et al. (2019). They also noted a direct linear correlation between Ea and lnA using the Coats – Redfern method, confirming the kinetic compensation phenomenon during thermal decomposition. The activation energy (Ea) and the pre-exponential factor (lnA), also referred to as the kinetic compensation effect (KCE), are known to correlate. This relationship can be described using the linear equation:

$$\ln A = a + bE \tag{12}$$

In this equation, a and b are constants determined from a specific set of experimental kinetic data. Specifically, a = lnK_iso and b = 1/(RT_iso), where T_ K_iso is the associated rate constant, and iso stands for the artificial isokinetic temperature. Figure 7 shows how lnA and Ea have a linear relationship values obtained using the Coats – Redfern (CR) method, as reported in Table 7. Table 8 further summarizes key KCE parameters including a, b, the correlation coefficient (R^2), K_iso, and T_iso (R. Chen et al. 2019). These insights are crucial for understanding the kinetic behavior of *FSSAW* fiber during pyrolysis and for selecting the most appropriate decomposition model.

Thermodynamics parameter analysis

The thermodynamic analysis of *FSSAW* fiber pyrolysis shown in Figure 8 offers a comprehensive view of the energy dynamics and reaction pathways that occur during biomass decomposition under varying heating rates. The observed highest enthalpy (ΔH) value of 249.65 kJ/mol at 50°C/min for Model 22 indicates that the process becomes more energy-demanding at higher temperatures. This is expected, as increased temperatures facilitate the breakdown of complex biomass structures but also require greater energy to overcome the activation energy barriers of chemical bonds (R. Chen et al. 2019). The highest Gibbs free energy (ΔG) value of 390.81 kJ/mol for Model 22 at 50°C/min further highlights the non-spontaneous nature of the pyrolysis reaction. As the temperature increases, the system requires more external energy to drive the reaction, demonstrating that pyrolysis is not a naturally occurring process but one that needs thermal input to proceed effectively (Ozyuguran, Akturk, and Yaman 2018b). The most negative entropy (ΔS) value of −0.31 kJ/mol·K for Model 13 at 30°C/min suggests that the transition state during pyrolysis is highly ordered compared to the initial biomass. This indicates that the molecular rearrangements occurring in the decomposition process result in a more structured and less disordered state, which is characteristic of solid-phase reactions (Ma et al. 2022). The negative values for entropy across all models reinforce the idea that pyrolysis is a process of molecular organization, with biomass undergoing significant structural changes that reduce its randomness. Overall, these results emphasize the complex interplay between enthalpy, Gibbs free energy, and entropy during *FSSAW* fiber pyrolysis. The process requires substantial external energy input, especially at higher temperatures, to overcome the reaction's lack of spontaneity. The negative entropy values highlight that the reaction leads to more ordered products, reflecting the typical nature of solid-phase decomposition (Pal et al. 2021). These

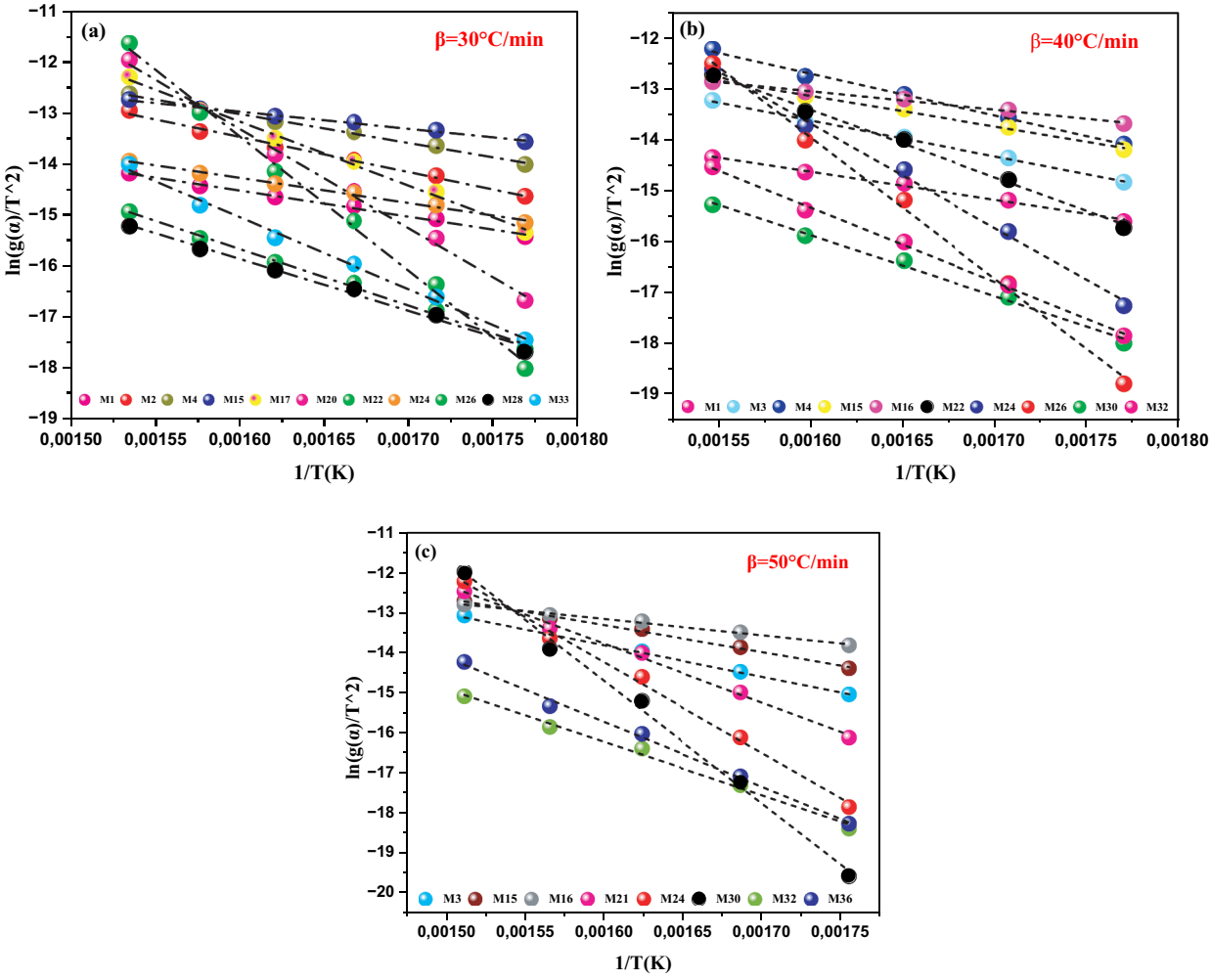

Figure 5. Fitting curves using the integral method to estimate the kinetic parameters of biomass pyrolysis with different diffusion and reaction order models.

findings not only provide valuable insights into the energetics of biomass pyrolysis but also serve as crucial information for optimizing the conditions under which pyrolysis can be most efficiently used for bioenergy production (Petrovič et al. 2023). By understanding these thermodynamic parameters, we can fine-tune the heating rates and other variables to achieve better conversion yields while minimizing energy consumption.

Kinetic comparison of criado's master plot on pyrolysis of FSSAW and coats-redfern

Several solid-state reaction models and Criado's master plot technique were used to examine the thermal degradation mechanism of *FSAAW* fibers (Khawam and Flanagan 2006), all of which exhibited high correlation coefficients ($R^2 > 0.99$) across the three studied heating rates. This method compares theoretical and experimental plots of the reduced conversion function g (α)/g(0.5) versus the degree of conversion (α), with experimental values derived from the DTG curves. Figure 9 shows the master curve plots g(α)/g(0.5) vs α for several mechanistic models using Criado's technique Among the tested models, the sigmoidal rate law, corresponding to Model *M*-16 (random nucleation and subsequent growth), showed the closest alignment with experimental data particularly within the conversion range of α = 0.15 to 0.55. This agreement suggests that the early stages of *FSAAW* pyrolysis are likely dominated by the formation of active centers followed by their expansion through the fiber matrix. However, beyond α = 0.55, significant deviations were observed, implying that a single-step reaction mechanism like that of Model *M*-16 becomes insufficient to accurately describe the decomposition process. This deviation indicates the emergence of more complex, multi-step pathways potentially involving diffusion, fragmentation, or secondary char-forming reactions. While

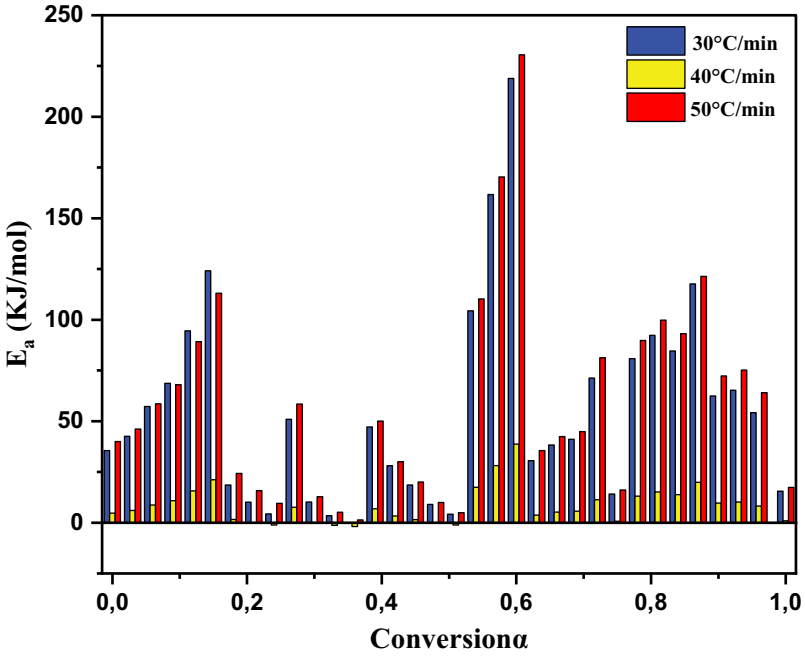

Figure 6. Activation energy ea versus conversion α.

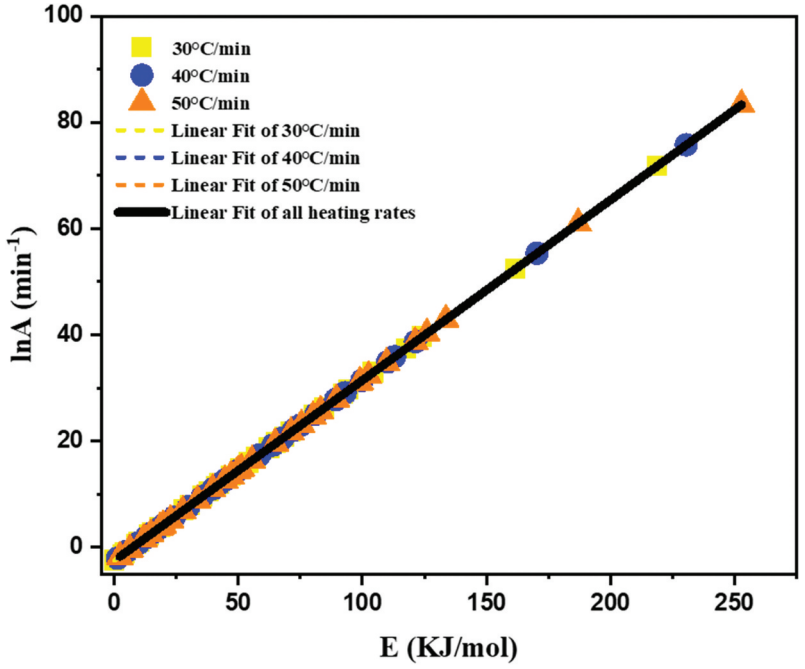

Figure 7. Isokinetic relationships (ln a vs. E) from the coats – Redfern method at different heating rates.

Criado's method is powerful due to its simplicity and direct use of experimental data, it does not yield precise values for activation energy (Ea) or the kinetic triplet (Ea, A, f(α)), limiting its utility for quantitative kinetic modeling (Ozyuguran, Akturk, and Yaman 2018a). Despite this limitation, the results obtained through Criado's master plot were consistent with those derived from the Coats – Redfern (CR) method, reinforcing the identification of an Advanced Reaction Model (ARN) and its Extended Geometrical Model (EGM) as suitable descriptors of *FSAAW* pyrolysis (Zikhali et al. 2023). These models point to radial diffusion in cylindrical particles as the rate-controlling step during the later stages of degradation. Such behavior supports the hypothesis of an expanding reaction front and highlights the necessity of

Table 7. Thermodynamic parameters of *FSSAW*..

Heating rate (°C/m)	30			40			50		
Model No.	ΔH kJ/mol	ΔG kJ/mol	ΔS kJ/mol. K	ΔH kJ/mol	ΔG kJ/mol	ΔS kJ/mol. K	ΔH kJ/mol	ΔG kJ/mol	ΔS kJ/mol. K
M-1	32.03	185.63	−0.25	36.98	178.20	−0.238	41.43	182.10	−0.24
M-2	39.35	191.55	−0.25	43.07	183.28	−0.236	48.10	187.63	−0.23
M-3	54.81	200.10	−0.24	55.55	190.02	−0.227	61.90	193.55	−0.22
M-4	66.70	203.12	−0.23	64.93	189.15	−0.210	72.36	204.03	−0.22
M-5	93.95	241.32	−0.24	86.07	222.82	−0.230	96.06	234.16	−0.23
M-6	125.00	274.90	−0.25	109.98	249.01	−0.234	122.87	262.83	−0.24
M-7	14.18	173.24	−0.26	21.27	166.68	−0.245	24.53	169.59	−0.24
M-8	5.32	168.45	−0.26	12.77	161.17	−0.250	15.59	163.54	−0.25
M-9	−0.80	167.49	−0.27	6.45	158.01	−0.255	8.99	159.78	−0.25
M-10	48.17	196.67	−0.24	55.35	190.36	−0.228	61.54	194.31	−0.22
M-11	5.43	168.62	−0.26	9.70	159.60	−0.252	11.65	161.27	−0.25
M-12	−1.68	167.79	−0.27	2.09	157.22	−0.261	3.34	157.93	−0.26
M-13	−5.24	184.29	−0.31	−1.71	160.68	−0.273	−0.82	159.55	−0.27
M-14	–	–	–						
M-15	44.18	193.19	−0.24	47.01	184.30	−0.231	52.45	188.38	−0.23
M-16	24.15	179.65	−0.25	26.97	170.54	−0.242	30.54	173.73	−0.24
M-17	14.13	173.11	−0.26	16.95	163.75	−0.247	19.58	166.11	−0.25
M-18	4.11	168.00	−0.27	6.93	158.21	−0.254	8.62	159.60	−0.25
M-19	−0.90	167.55	−0.27	1.91	157.16	−0.261	3.15	157.84	−0.26
M-20	104.28	250.91	−0.24	107.15	244.47	−0.231	118.18	256.62	−0.23
M-21	164.38	312.51	−0.25	167.28	306.94	−0.235	183.91	324.34	−0.24
M-22	224.49	371.38	−0.25	227.42	367.91	−0.237	249.65	390.81	−0.24
M-23	–	–	–						
M-24	26.80	181.79	−0.25	32.52	174.80	−0.240	36.60	178.42	−0.24
M-25	34.86	187.80	−0.25	39.35	180.09	−0.237	44.02	184.15	−0.24
M-26	37.82	190.16	−0.25	41.81	182.15	−0.236	46.71	186.39	−0.24
M-27	69.54	202.61	−0.22	78.17	208.54	−0.220	86.48	220.12	−0.23
M-28	9.47	170.67	−0.26	13.11	161.60	−0.250	15.37	163.64	−0.25
M-29	79.52	218.27	−0.23	86.75	219.65	−0.224	95.78	230.89	−0.23
M-30	91.57	232.80	−0.23	96.73	230.24	−0.225	106.71	242.25	−0.23
M-31	83.51	216.76	−0.22	90.06	220.97	−0.221	99.40	233.32	−0.23
M-32	118.16	264.38	−0.24	118.33	255.31	−0.231	130.56	268.73	−0.23
M-33	60.21	208.16	−0.24	69.25	203.45	−0.226	77.00	208.36	−0.22
M-34	63.21	210.06	−0.24	72.12	204.76	−0.224	80.04	208.30	−0.22
M-35	51.62	202.28	−0.25	60.96	198.41	−0.232	68.18	204.25	−0.23
M-36	10.95	171.56	−0.26	14.34	162.43	−0.249	16.71	164.58	−0.25

Table 8. Relevant parametric values for the "kinetic compensation effect".

Heating rate (°C/min)	a (min^{-1})	95% CI for a	b (mol/kJ)	95% CI for b	k_{iso}	T_{iso} (°C)	R^2
30	−3.2345	(−3.8901, −2.5790)	0.3556	(0.3532, 0.3580)	0.0212	342.567	0.99
40	−1.8963	(−2.6174, −1.1752)	0.3445	(0.3421, 0.3470)	0.1254	352.210	0.99
50	−1.5438	(−2.2664, −0.8211)	0.3321	(0.3298, 0.3344)	0.1602	364.753	0.99
Combination of all heating rates	−2.3340	(−2.5759, −2.0921)	0.3412	(0.3397, 0.3426)	0.1143	353.482	0.99

incorporating geometrical and transport constraints into the modeling of lignocellulosic biomass pyrolysis. Ultimately, the integration of both Criado's and CR methods enhances the reliability of mechanistic interpretation and underscores the complexity of *FSAAW* fiber degradation.

Practical implications of FSSAW fiber pyrolysis

Economic efficiency

The pyrolytic conversion of FSSAW fibers demonstrates promising economic viability. Agave americana stalks are an agricultural byproduct, typically discarded after flowering. This makes the raw material low-cost and abundantly available, particularly in semi-arid and arid regions where Agave thrives. The simple extraction process soaking, manual retting, and drying does not require expensive chemical treatments or high-tech machinery, significantly reducing preprocessing costs. Furthermore, the high volatile matter content (76.85%) and low ash residue (2.31%) enhance the bio-oil yield, making FSAAW a suitable feedstock for fuel-grade pyrolysis products. The elevated higher heating value (HHV = 19.25 MJ/kg) supports its use as an energy-rich biomass. Collectively, these characteristics reduce the cost-per-MJ of energy produced and may lead to favorable return on investment (ROI) in decentralized bioenergy systems.

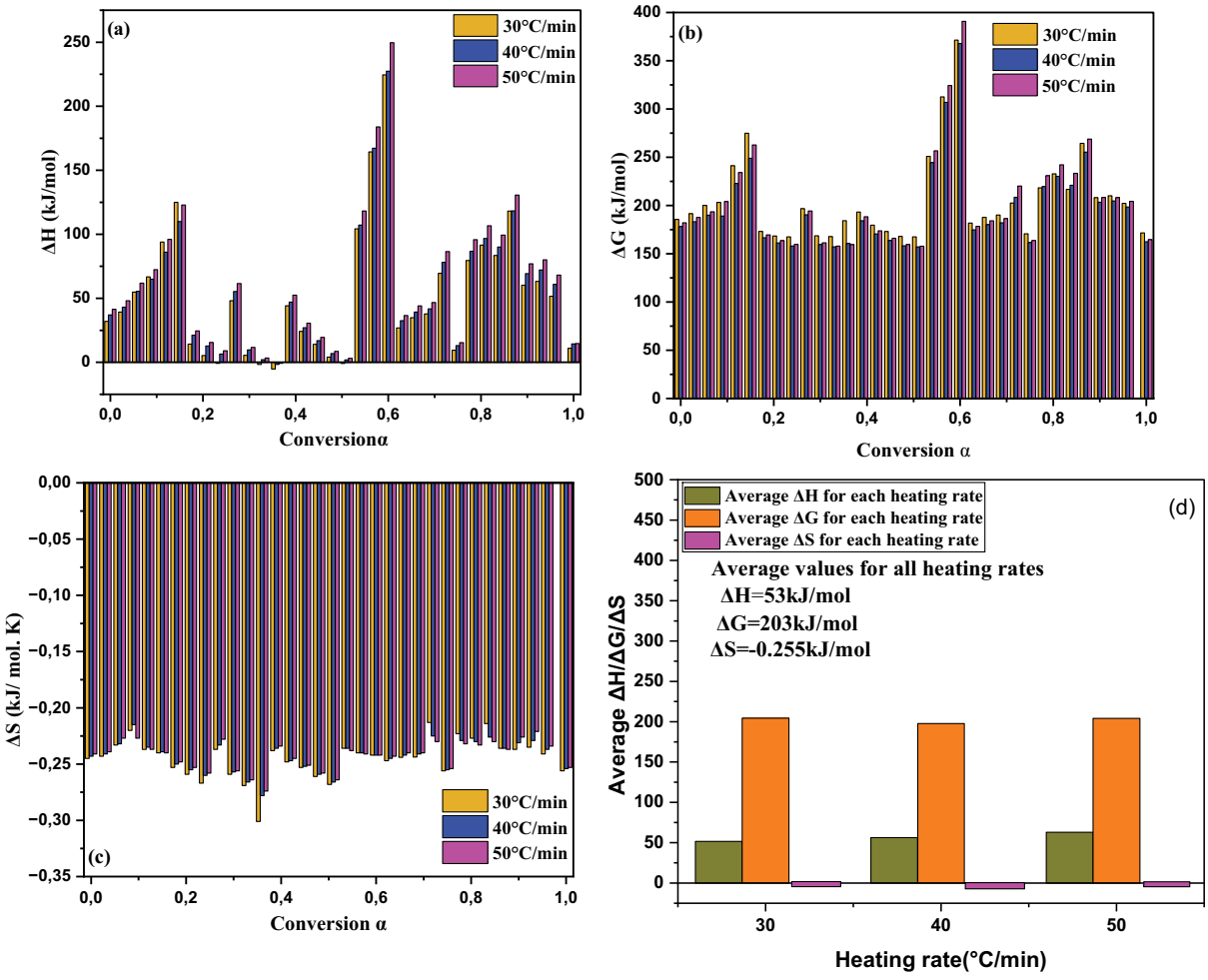

Figure 8. The variations of ΔH, ΔG, ΔS with conversion rate (α) and ?.

Scalability of the process

The scalability of the pyrolysis process using FSAAW fibers is favorable due to the simplicity of the thermal decomposition stages and the availability of agave stalks. The thermal behavior observed (distinct decomposition zones for hemicellulose, cellulose, and lignin) enables modular reactor design, allowing for flexible scaling from lab-scale batch reactors to continuous pilot or industrial-scale systems. The kinetic analysis, which includes Coats – Redfern and Criado's master plots, provides a comprehensive mechanistic understanding, allowing the design of process controls and reactor conditions that are adaptable to large-scale applications. In regions with high Agave cultivation, especially North Africa, Latin America, and the Mediterranean, biomass aggregation centers can be developed to supply feedstock to centralized or distributed pyrolysis units, enabling regional bioenergy deployment.

Environmental impact and sustainability

Environmentally, the use of FSAAW fibers as feedstock aligns well with the principles of circular economy and biowaste valorization. Converting agricultural waste into bioenergy reduces open-field burning or landfilling, thus cutting down methane and CO_2 emissions. The slow decomposition of lignin and high char residue yield also support biochar production, which can be used as a soil amendment to sequester carbon and improve soil fertility. Additionally, the absence of toxic additives or pretreatment chemicals during fiber preparation ensures minimal ecotoxicity. As an added benefit, replacing fossil fuels with FSAAW-derived bio-oil or syngas can significantly lower lifecycle greenhouse gas (GHG) emissions. However, sustainability should also consider water

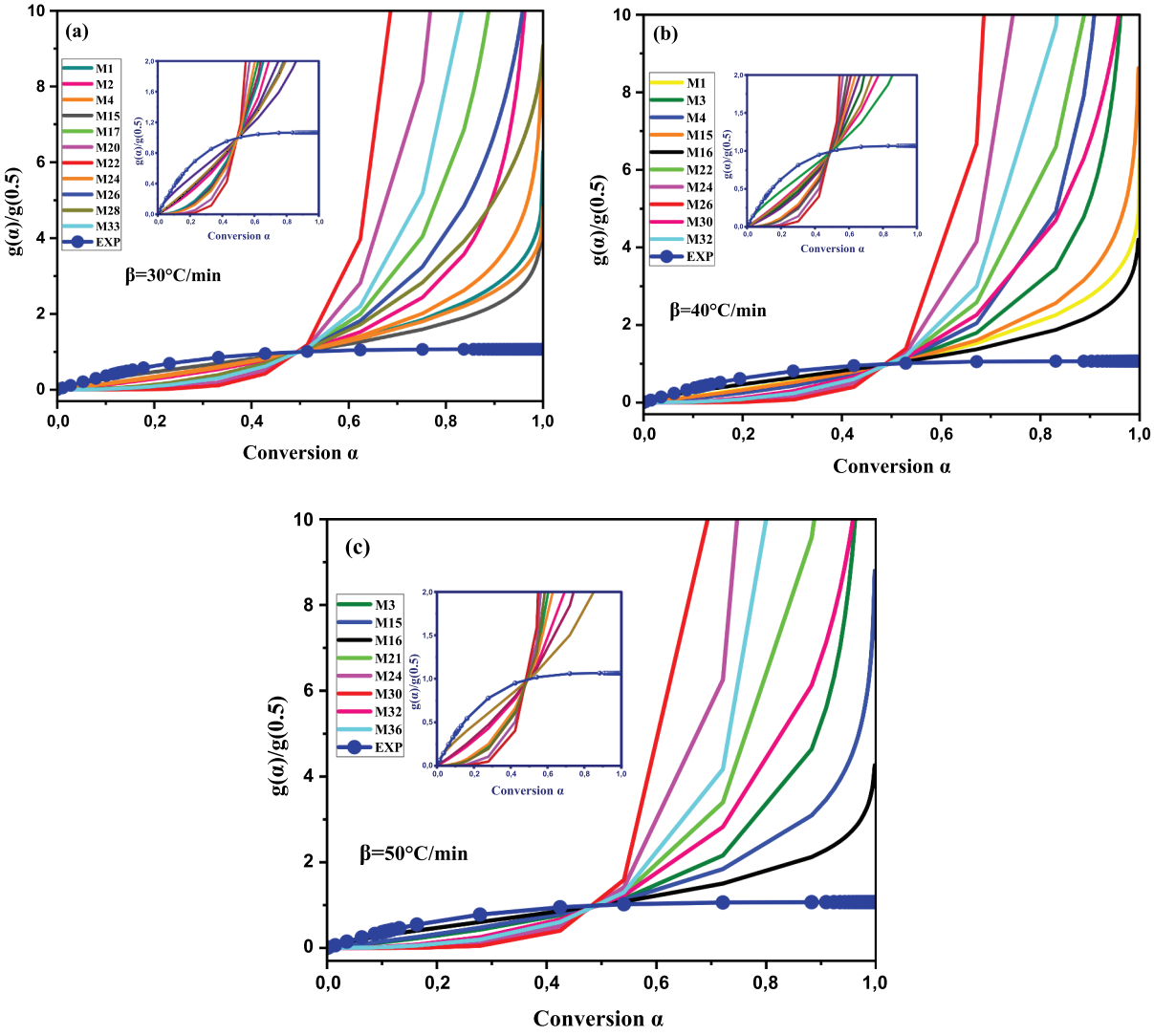

Figure 9. Criado's master plot of *FSSAW* at 30, 40, and 50 °C/min.

use during soaking and the energy balance of drying operations. To mitigate this, integrating solar drying or passive evaporation and anaerobic soaking tanks can reduce the ecological footprint of the process.

Practical recommendations

To advance this research, future studies should apply model-free isoconversional methods such as Flynn – Wall – Ozawa or Vyazovkin to validate activation energies across varying conversion levels. Pilot-scale pyrolysis trials are essential to evaluate the practical performance of FSSAW under dynamic operating conditions. Additionally, exploring catalyst-assisted pyrolysis could help reduce activation energy and enhance biofuel yields. Advanced analyses using coupled techniques like TGA-FTIR or TGA-GC-MS would offer insights into reaction intermediates and gaseous products, improving the understanding and control of decomposition pathways. From an application standpoint, the FSSAW fiber's high volatile content (76.85%), low ash (2.31%), and significant HHV (19.25 MJ/kg) make it a strong candidate for fast pyrolysis or gasification processes. Its composition is well-suited for producing bio-oil and biochar, supporting renewable energy systems, soil carbon sequestration, and circular bioeconomy strategies. Moreover, insights into its kinetic and thermodynamic behaviors enable more accurate reactor design, better process control, and scalable bioenergy solutions.

Conclusion

This study comprehensively investigated the pyrolysis behavior and kinetic characteristics of FSAAW (Flower Stalk of Agave Americana Waste) fibers to evaluate their potential for bioenergy production. The thermal degradation process was characterized under varying heating rates (30°C, 40°C, and 50°C/min), and key kinetic and thermodynamic parameters were quantified using the Coats – Redfern method alongside mechanistic analysis.

The main findings are summarized as follows:

- FSAAW fibers exhibit a multi-stage pyrolytic degradation corresponding to their chemical composition, with cellulose, hemicellulose, and lignin decomposing distinctly across the temperature range of approximately 200–800°C.
- Increasing the heating rate from 30°C to 50°C/min shifted the degradation temperatures higher, consistent with a thermal lag effect.
- The activation energy (Ea) was found to increase with heating rate, ranging from 218.87 kJ/mol at 30 °C/min to 252.73 kJ/mol at 50 °C/min (Model M22), indicating that greater energy is required for decomposition at faster heating.
- The kinetic compensation effect (KCE) was confirmed by a strong linear correlation (R^2 ≈0.99) between lnA and Ea, reflecting the interplay between activation energy and molecular collision frequency.
- Thermodynamic analysis revealed the pyrolysis reaction to be non-spontaneous, with a maximum Gibbs free energy change (ΔG) of 390.81 kJ/mol, and an enthalpy change (ΔH) peaking at 249.65 kJ/mol, while the negative entropy change (ΔS) of −0.31 kJ/mol·K suggested the formation of more ordered products during decomposition.
- Mechanistic evaluation using Criado's master plot identified a sigmoidal rate law (Model M16) governing early-stage pyrolysis (α = 0.15–0.55), with radial diffusion controlling the later stages, indicating increasingly complex, multi-step reaction pathways.

These insights into FSAAW fiber pyrolysis kinetics and thermodynamics provide a foundation for optimizing pyrolysis conditions to maximize bioenergy yield and efficiency. Future studies should focus on refining operational parameters and exploring reactor designs to harness the full bioenergy potential of FSAAW fibers.

Acknowledgments

The authors are thankful to the Deanship of Graduate Studies and Scientific Research at Najran University for funding this work under the Growth Funding Program grant code (NU/GP/SERC/13/40-5).

Disclosure statement

No potential conflict of interest was reported by the author(s).

ORCID

Ahmed Belaadi http://orcid.org/0000-0002-6059-3974

Nomenclature and abbreviation

TGA	Thermogravimetric analysis
FTIR	Fourier Transform Infrared
PEFS	Perkin Elmer Frontier Spectroscopy
f(α)	Function of reaction mechanism (differential form)
g(α)	Function of reaction mechanism (integral form)
β	Heating rate
Ea	Activation energy
h	Planck constant (6.626×10^{23})
K^B	Boltzmann constant (1.381×10^{23})
R	Universal gas constant (8.314)
A	Pre-exponential factor
ΔH	Enthalpy change
ΔG	Gibbs free energy change
ΔS	Entropy change
T	Temperature
T_P	Peak temperature
α	Degree of conversion
x	Dimensionless activation parameter: Ea/(R·T)
W_0	Initial sample weight
W_f	Weight at time t
Wf	Final sample weight
M	Kinetic model
ARN	Assumed Random Nucleation
EGM	Ensuing Growth Model

References

Agnihotri, N., and M. Kumar. 2024. "Thermal Analysis, Kinetic Behavior, Reaction Modeling, and Comprehensive Pyrolysis Index of Soybean Stalk Pyrolysis, Biomass Convers." *Biomass Conversion and Biorefinery* 14 (13): 14977–14992. https://doi.org/10.1007/s13399-023-03807-8.

Ali, I., R. Tariq, S. R. Naqvi, A. H. Khoja, M. T. Mehran, M. Naqvi, and N. Gao. 2021. "Kinetic and Thermodynamic Analyses of Dried Oily Sludge Pyrolysis." *Journal of the Energy Institute* 95:30–40. https://doi.org/10.1016/j.joei.2020.12.002.

Ali, I., R. Tariq, S. Raza, A. Hussain, M. Taqi, M. Naqvi, and N. Gao. 2021. "Kinetic and Thermodynamic Analyses of Dried Oily Sludge Pyrolysis." *Journal of the Energy Institute* 95:30–40. https://doi.org/10.1016/j.joei.2020.12.002.

Alves, J. L. F., J. C. G. da Silvada Silva, V. F. da Silva Filho, R. F. Alves, W. V. de Araujo Galdino, and R. F. De Sena. 2019. "Kinetics and Thermodynamics Parameters Evaluation of Pyrolysis of Invasive Aquatic Macrophytes to Determine Their Bioenergy Potentials." *Biomass and Bioenergy* 121:28–40. https://doi.org/10.1016/j.biombioe.2018.12.015.

Anca-Couce, A., C. Tsekos, S. Retschitzegger, F. Zimbardi, A. Funke, S. Banks, T. Kraia, et al. 2020. "Biomass Pyrolysis TGA Assessment with an International Round Robin." *Fuel* 276:118002. https://doi.org/10.1016/j.fuel.2020.118002.

Apaydın Varol, E., and Ü. Mutlu. 2023. "Department, tga-Ftir Analysis of Biomass Samples Based on the Thermal." *Energ* 16. https://doi.org/10.3390/en16093674.

Ballesteros, L. F., J. A. Teixeira, and S. I. Mussatto. 2014. "Chemical, Functional, and Structural Properties of Spent Coffee Grounds and Coffee Silverskin." *Food and Bioprocess Technology* 7 (12): 3493–3503. https://doi.org/10.1007/s11947-014-1349-z.

Bourmaud, A., and C. Baley. 2010. "Effects of Thermo Mechanical Processing on the Mechanical Properties of Biocomposite Flax Fibers Evaluated by Nanoindentation." *Polymer Degradation & Stability* 95:1488–1494. https://doi.org/10.1016/j.polymdegradstab.2010.06.022.

Chen, C. 2020. "Thermal Decomposition and Kinetics Analysis of Microwave Pyrolysis of Dunaliella Salina Using Composite Additives." *BioEnergy Research* 13 (4): 1205–1220. https://doi.org/10.1007/s12155-020-10150-7.

Chen, R., Q. Li, X. Xu, and D. Zhang. 2019. "Pyrolysis Kinetics and Reaction Mechanism of Representative Non-Charring Polymer Waste with Micron Particle Size, Energy Convers." *Energy Conversion and Management* 198:111923. https://doi.org/10.1016/j.enconman.2019.111923.

Constantino, J., S. Layara, F. Andersen, R. Lucio, R. De Fatima, P. Muniz, and H. J. Jos. 2019. "Biomass and Bioenergy Bioenergetic Potential of Ponkan Peel Waste (citrus Reticulata) Pyrolysis by Kinetic Modelling and Product Characterization." *Biomass and Bioenergy* 131:105401. https://doi.org/10.1016/j.biombioe.2019.105401.

Dewayanto, N., R. Isha, and M. Ridzuan. 2014. "Kinetic Study on the Catalytic Pyrolysis of Decanter Cake from Palm Oil Milling Plant by Using Thermogravimetry Data." *Jurnal Teknologi* 5 (5): 65–69. https://doi.org/10.11113/jt.v69.3207.

Dhaundiyal, A., S. B. Singh, M. M. Hanon, and R. Rawat. 2018. "Determination of Kinetic Parameters for the Thermal Decomposition of Parthenium Hysterophorus." *Rigas Tehniskas Universitates Zinatniskie Raksti* 22 (1): 5–21. https://doi.org/10.1515/rtuect-2018-0001.

Ding, Y., B. Huang, C. Wu, Q. He, and K. Lu. 2019. "Kinetic Model and Parameters Study of Lignocellulosic Biomass Oxidative Pyrolysis." *Energy* 181:11–17. https://doi.org/10.1016/j.energy.2019.05.148.

Dubdub, I., and M. Al-Yaari. 2020. "Pyrolysis of Low Density Polyethylene: Kinetic Study Using TGA Data and ANN Prediction." *Polymers* 12 (4): 891. https://doi.org/10.3390/polym12040891.

El, S. A., S. Tarek, and M. K. Mohamed. 2024. "Thermal Degradation Behaviour and Chemical Kinetic Characteristics of Biomass Pyrolysis Using TG/DTG/DTA Techniques, Biomass Convers." *Biomass Conversion and Biorefinery* 14 (15): 17779–17803. https://doi.org/10.1007/s13399-023-03926-2.

Elmay, Y., M. Jeguirim, G. Trouvé, and R. Said. 2016. "Environmental Effects Kinetic Analysis of Thermal Decomposition of Date Palm Residues Using Coats – Redfern Method." *Energy Sources* 38 (8): 7036. https://doi.org/10.1080/15567036.2013.821547.

Estrada, M., D. L. Linero, and F. Ramírez. 2013. "Constitutive Relationship of the Fiber Cluster of Bamboo Guadua Angustifolia, Determined by Means of a Weibull Probability Function and a Model of Progressive Failure." *Mechanics of Materials: An International Journal* 63:12–20. https://doi.org/10.1016/j.mechmat.2013.04.007.

Felipe, F., D. A. Ferreira, F. José, Q. Monte, T. Leda, and G. De Lemos. 2017. "Synthesis of Chiral Esters and Alcohols via Enantioselective Esterification with Citrus Aurantium Peels as Biocatalyst, Ind." *Industrial Crops and Products* 96:23–29. https://doi.org/10.1016/j.indcrop.2016.11.013.

Ferfari, O., A. Belaadi, M. Bourchak, D. Ghernaout, and R. M. Ajaj. 2024. "Thermal Decomposition of Syagrus Romanzoffiana Palm Fibers: Thermodynamic and Kinetic Studies Using the Coats-Redfern Method." *Energy* 231:120928. https://doi.org/10.1016/j.renene.2024.120928.

Gayathri, K., K. Rajesh, P. Krishnan, K. Anandan, R. Swadhi, A. R. Devaraj, and G. Anbalagan. 2020. "A Study on Kinetic Properties of Brucinium Hydrogen (S) Malate Pentahydrate Single Crystal by Coats Redfern Method." *AIP Conference Proceedings* 2265. https://doi.org/10.1063/5.0017481.

Gerald Arul Selvan, M. T., J. S. Binoj, B. B. Mansingh, and J. A. Baby Sajin. 2023. "physico-Chemical Properties of Alkali Treated Cellulosic Fibers from Pine Prop Root." *Journal of Natural Fibers* 20 (1): 148–161. https://doi.org/10.1080/15440478.2022.2129897.

Goumghar, A., M. Assarar, W. Zouari, K. Azouaoui, A. El Mahi, and R. Ayad. 2022. "Study of the Fatigue Behaviour of Hybrid Flax-Glass/epoxy Composites." *Composite Structures* 294:115790. https://doi.org/10.1016/j.compstruct.2022.115790.

Gourier, C., A. Le Duigou, A. Bourmaud, and C. Baley. 2014. "Mechanical Analysis of Elementary Flax Fibre Tensile Properties After Different Thermal Cycles, Compos. Part a Appl." *Applied Science & Manufacturing* 64:159–166. https://doi.org/10.1016/j.compositesa.2014.05.006.

Gupta, A., S. K. Thengane, and S. Mahajani. 2020. "Kinetics of Pyrolysis and Gasification of Cotton Stalk in the Central Parts of India." *Fuel* 263:116752. https://doi.org/10.1016/j.fuel.2019.116752.

Gurukarthik Babu, B., D. Prince Winston, P. SenthamaraiKannan, S. S. Saravanakumar, and M. R. Sanjay. 2019. "Study on Characterization and Physicochemical Properties of New Natural Fiber from Phaseolus Vulgaris." *Journal of Natural Fibers* 16 (7): 1035–1042. https://doi.org/10.1080/15440478.2018.1448318.

Hameed, Z., Z. Aman, S. R. Naqvi, R. Tariq, I. Ali, and A. A. Makki. 2018. "Kinetic and Thermodynamic Analyses of Sugar Cane Bagasse and Sewage Sludge Co-Pyrolysis Process." *Energy and Fuels* 32 (9): 9551–9558. https://doi.org/10.1021/acs.energyfuels.8b01972.

Hu, B., Z. Gu, J. Su, and Z. Li. 2021. "Pyrolytic Characteristics and Kinetics of Guanzhong Wheat Straw and Its Components for High-Value Products." *BioResources* 16 (1): 1958–1979. https://doi.org/10.15376/biores.16.1.1958-1979.

Huang, H., J. Liu, H. Liu, F. Evrendilek, and M. Buyukada. 2020. "Pyrolysis of Water Hyacinth Biomass Parts: Bioenergy, Gas Emissions, and By-Products Using tg-Ftir and py-Gc/ms Analyses." *Energy Convers managenergy Conversion and Management* 207:112552. https://doi.org/10.1016/j.enconman.2020.112552.

Inayat, A., F. Jamil, S. F. Ahmed, M. Ayoub, P. M. Abdul, M. Aslam, M. Mofijur, Z. Khan, and A. Mustafa. 2023. "Thermal Degradation Characteristics, Kinetic and Thermodynamic Analyses of Date Palm Surface Fibers at Different Heating Rates." *Fuel* 335:127076. https://doi.org/10.1016/j.fuel.2022.127076.

Inayat, A., F. Jamil, S. Forruque, M. Ayoub, P. Mohamed, M. Aslam, M. Mofijur, Z. Khan, and A. Mustafa. 2023. "Thermal Degradation Characteristics, Kinetic and Thermodynamic Analyses of Date Palm Surface Fibers at Different Heating Rates." *Fuel* 335:127076. https://doi.org/10.1016/j.fuel.2022.127076.

Khawam, A., and D. R. Flanagan. 2006. "Solid-State Kinetic Models: Basics and Mathematical Fundamentals." *The Journal of Physical Chemistry: B* 110 (35): 17315–17328. https://doi.org/10.1021/jp062746a.

Klinger, J. L., T. L. Westover, R. M. Emerson, C. L. Williams, S. Hernandez, G. D. Monson, and J. C. Ryan. 2018. "Effect of Biomass Type, Heating Rate, and Sample Size on Microwave-Enhanced Fast Pyrolysis Product Yields and Qualities, Appl." *Applied Energy* 228:535–545. https://doi.org/10.1016/j.apenergy.2018.06.107.

Komandur, J., R. Vinu, and K. Mohanty. 2022. "Pyrolysis Kinetics and Pyrolysate Composition Analysis of Mesua Ferrea L: A Non-Edible Oilseed Towards the Production of Sustainable Renewable Fuel." *Bioresource Technology* 351:126987. https://doi.org/10.1016/J.BIORTECH.2022.126987.

Kumar, M., D. Rai, G. Bhardwaj, S. N. Upadhyay, and P. K. Mishra. 2021. "Pyrolysis of Peanut Shell: Kinetic Analysis and Optimization of Thermal Degradation Process, Ind." *Crops Production* 174:114128. https://doi.org/10.1016/j.indcrop.2021.114128.

Lalaymia, I., A. Bedjaoui, A. Belaadi, M. M. S. Abdullah, D. Ghernaout, and A. Al-Khawlani. 2024. "Slow Pyrolysis of Agave Americana L. Fibers: Analysis of Kinetics and Thermodynamics Using the Coats-Redfern Method at Different Heating Rates." *Industrial Crops and Products* 219:119043. https://doi.org/10.1016/j.indcrop.2024.119043.

Lalaymia, I., A. Belaadi, A. Bedjaoui, H. Alshahrani, and M. K. A. Khan. 2023. "Extraction and Characterization of Fiber from the Flower Stalk of the Agave Plant for Alternative Reinforcing Biocomposite Materials." *Biomass Convers Biorefinery* 14 (24): 32271–32287. https://doi.org/10.1007/s13399-023-04782-w.

Lalaymia, I., A. Belaadi, M. Boumaaza, H. Alshahrani, M. K. A. Khan, and A. Dib. 2024. "Weibull Statistic and Artificial Neural Network Analysis of the Mechanical Performances of Fibers from the Flower Agave Plant for eco-Friendly Green Composites." *Journal of Natural Fibers* 21 (1). https://doi.org/10.1080/15440478.2024.2305228.

Lalaymia, I., A. Belaadi, and D. Ghernaout. 2025. "Biomass and Bioenergy Studying Gaussian Deconvolution and Multicomponent Kinetics Models in Agave Cellulosic Fibers Pyrolysis: Application in Sustainable Bioenergy for Cleaner Production." *Biomass and Bioenergy* 192:107488. https://doi.org/10.1016/j.biombioe.2024.107488.

Lei, J., X. Ye, H. Wang, and D. Zhao. 2023. "Insights into Pyrolysis Kinetics, Thermodynamics, and the Reaction Mechanism of Wheat Straw for Its Resource Utilization." *Sustainability* 15 (16): 12536. https://doi.org/10.3390/su151612536.

Lemoine, F., I. Maupin, L. Lemée, J. Lavoie, J. Lemberton, Y. Pouilloux, and L. Pinard. 2013. "Bioresource Technology Alternative Fuel Production by Catalytic Hydroliquefaction of Solid Municipal Wastes, Primary Sludges and Microalgae." *Bioresource Technology* 142:1–8. https://doi.org/10.1016/j.biortech.2013.04.123.

Li, W., Q. Dang, R. C. Brown, D. Laird, and M. M. Wright. 2017. "Bioresource Technology the Impacts of Biomass Properties on Pyrolysis Yields, Economic and Environmental Performance of the Pyrolysis-Bioenergy-Biochar Platform to Carbon Negative Energy." *Bioresource Technology* 241:959–968. https://doi.org/10.1016/j.biortech.2017.06.049.

Loy, A. C. M., D. K. W. Gan, S. Yusup, B. L. F. Chin, M. K. Lam, M. Shahbaz, P. Unrean, M. N. Acda, and E. Rianawati. 2018. "Thermogravimetric Kinetic Modelling of in-Situ Catalytic Pyrolytic Conversion of Rice Husk to Bioenergy Using Rice Hull Ash Catalyst." *Bioresource Technology* 261:213–222. https://doi.org/10.1016/j.biortech.2018.04.020.

Ma, C., F. Zhang, J. Hu, H. Wang, S. Yang, and H. Liu. 2023. "Co-Pyrolysis of Sewage Sludge and Waste Tobacco Stem: Gas Products Analysis, Pyrolysis Kinetics, Artificial Neural Network Modeling, and Synergistic Effects." *Bioresource Technology* 389:129816. https://doi.org/10.1016/j.biortech.2023.129816.

Ma, C., F. Zhang, H. Liu, H. Wang, and J. Hu. 2022. "Thermogravimetric Pyrolysis Kinetics Study of Tobacco Stem via Multicomponent Kinetic Modeling, Asym2sig Deconvolution and Combined Kinetics." *Bioresource Technology* 360:127539. https://doi.org/10.1016/j.biortech.2022.127539.

Naqvi, S. R., Y. Uemura, N. Osman, and S. Yusup. 2015. "Kinetic Study of the Catalytic Pyrolysis of Paddy Husk by Use of Thermogravimetric Data and the coats-Redfern Model." *Research on Chemical Intermediates* 41 (12): 9743–9755. https://doi.org/10.1007/s11164-015-1962-0.

Navarro, M. V., J. M. López, A. L. Veses, M. S. Callén, and T. García. 2018. "Kinetic Study for the Co-Pyrolysis of Lignocellulosic Biomass and Plastics Using the Distributed Activation Energy Model." *Energy* 165:731–742. https://doi.org/10.1016/j.energy.2018.09.133.

Ni, Z., H. Bi, C. Jiang, C. Wang, J. Tian, W. Zhou, H. Sun, and Q. Lin. 2021. "Investigation of the Co-Pyrolysis of Coal Slime and Coffee Industry Residue Based on Machine Learning Methods and tg-Ftir: Synergistic Effect, Kinetics and Thermodynamic." *Fuel* 305:121527. https://doi.org/10.1016/j.fuel.2021.121527.

Ozyuguran, A., A. Akturk, and S. Yaman. 2018a. "Optimal Use of Condensed Parameters of Ultimate Analysis to Predict the Calori Fi C Value of Biomass." *Fuel* 214:2361. https://doi.org/10.1016/j.fuel.2017.10.082.

Ozyuguran, A., A. Akturk, and S. Yaman. 2018b. "Optimal Use of Condensed Parameters of Ultimate Analysis to Predict the Calorific Value of Biomass." *Fuel* 214:640–646. https://doi.org/10.1016/j.fuel.2017.10.082.

Pal, D. B., N. Srivastava, S. L. Pal, M. Kumar, A. Syed, A. M. Elgorban, R. Singh, and V. K. Gupta. 2021. "Lignocellulosic Composition Based Thermal Kinetic Study of Mangiferaindica Lam, Artocarpus Heterophyllus Lam and Syzygium Jambolana Seeds." *Bioresource Technology* 341:125891. https://doi.org/10.1016/j.biortech.2021.125891.

Parida, P. K., A. K. Pradhan, and M. K. Pandit. 2023. "Characterization of Cellulose Fiber Extracted from Stems of Myriostachya Wightiana (MW) Plants: A Viable Reinforcement for Polymer Composite." *Fibers and Polymers* 24:489–503. https://doi.org/10.1007/s12221-023-00020-2.

Petrovič, A., J. Stergar, L. Škodič, N. Rašl, T. C. Predikaka, L. Čuček, D. Goričanec, and D. Urbancl. 2023. "Thermo-Kinetic Analysis of Pyrolysis of Thermally Pre-Treated Sewage Sludge from the Food Industry." *Thermal Science and Engineering Progress* 42:101863. https://doi.org/10.1016/j.tsep.2023.101863.

Postawa, K., H. Fa, J. Szczygie, E. Beran, and M. Kułażyński. 2022. "Bioresource Technology Analyzing the Kinetics of Waste Plant Biomass Pyrolysis via Thermogravimetry Modeling and Semi-Statistical Methods." *Bioresource Technology* 344:126181. https://doi.org/10.1016/j.biortech.2021.126181.

Raza, M., B. Abu-Jdayil, A. H. Al-Marzouqi, and A. Inayat. 2022. "Inayat, Kinetic and Thermodynamic Analyses of Date Palm Surface Fibers Pyrolysis Using coats-Redfern Method." *Renewable Energy* 183:67–77. https://doi.org/10.1016/j.renene.2021.10.065.

Raza, S., R. Tariq, Z. Hameed, I. Ali, M. Naqvi, W. Chen, S. Ceylan, et al. 2019. "Pyrolysis of High Ash Sewage Sludge: Kinetics and Thermodynamic Analysis Using coats-Redfern Method." *Renewable Energy* 131:131. https://doi.org/10.1016/j.renene.2018.07.094.

Saddawi, A., J. M. Jones, and A. Williams. 2012. "In Fl Uence of Alkali Metals on the Kinetics of the Thermal Decomposition of Biomass, Fuel Process." *Fuel Processing Technology* 104:189–197. https://doi.org/10.1016/j.fuproc.2012.05.014.

Salama, S. 2020. "A Complete Characterization of Microalgal Biomass Through FTIR/TGA/CHNS Analysis: An Approach for Biofuel Generation and Nutrients Removal." *Renewable Energy*. https://doi.org/10.1016/j.renene.2020.10.066.

Sarkar, J. K., and Q. Wang. 2020. "Characterization of Pyrolysis Products and Kinetic Analysis of Waste Jute Stick Biomass." *Processes* 8 (7): 837. https://doi.org/10.3390/pr8070837.

Selvan, M. T. G. A., J. S. Binoj, J. T. E. J. Moses, N. P. Sai, S. Siengchin, M. R. Sanjay, and Y. Liu. 2022. "Extraction and Characterization of Natural Cellulosic Fiber from Fragrant Screw Pine Prop Roots as Potential Reinforcement for Polymer Composites." *Polymer Composites* 43 (1): 320–329. https://doi.org/10.1002/pc.26376.

Shagali, A. A., M. E. Mostafa, H. Li, S. Hu, J. Xu, L. Jiang, Y. Wang, S. Su, and J. Xiang. 2023. "Pyrolysis Characteristics and Kinetic Parameters Assessment of Typical Agricultural Residues Using High Heating Photothermal TGA." *Journal of Analytical and Applied Pyrolysis* 174:106109. https://doi.org/10.1016/j.jaap.2023.106109.

Sharifzadeh, M., M. Sadeqzadeh, M. Guo, T. N. Borhani, N. V. S. N. Murthy Konda, M. C. Garcia, L. Wang, J. Hallett, and N. Shah. 2019. "The Multi-Scale Challenges of Biomass Fast Pyrolysis and Bio-Oil Upgrading: Review of the State of Art and Future Research Directions, Prog." *Energy and Combustion Science* 71:1–80. https://doi.org/10.1016/j.pecs.2018.10.006.

Sharma, R., A. Joshi, and G. P. Singh. n.d. "TGA and Thermal Kinetics of Raw Calotropis Procera Fiber Reinforced PF Composites." *Journal of Condensed Matter* 1 (1): 24–27. https://doi.org/10.61343/jcm.v1i01.6.

Stamopoulos, A. G., K. I. Tserpes, and A. J. Dentsoras. 2018. "Quality Assessment of Porous CFRP Specimens Using x-Ray Computed Tomography Data and Artificial Neural Networks." *Composite Structures* 192:327–335. https://doi.org/10.1016/j.compstruct.2018.02.096.

Sun, Y., and J. Cheng. 2002. "Hydrolysis of Lignocellulosic Materials for Ethanol Production: A Review Q." *Bioresource Technology* 83 (1): 1–11. https://doi.org/10.1016/S0960-8524(01)00212-7.

Torres-Sciancalepore, R., A. Fernandez, D. Asensio, M. Riveros, M. P. Fabani, G. Fouga, R. Rodriguez, and G. Mazza. 2022. "Kinetic and Thermodynamic Comparative Study of Quince Bio-Waste Slow Pyrolysis Before and After Sustainable Recovery of Pectin Compounds." *Energy Convers managenergy Conversion and Management* 252:115076. https://doi.org/10.1016/J.ENCONMAN.2021.115076.

V, E. S. P. B., J. M. Criado, J. Malek, and A. Ortega. 1989. "Applicability of the Master Plots in Kinetic Analysis." *Thermochimica Acta* 147 (2): 377–385. https://doi.org/10.1016/0040-6031(89)85192-5.

Van De Velden, M., J. Baeyens, A. Brems, B. Janssens, and R. Dewil. 2010. "Fundamentals, Kinetics and Endothermicity of the Biomass Pyrolysis Reaction." *Renewable Energy* 35 (1): 232–242. https://doi.org/10.1016/j.renene.2009.04.019.

Vieira, B. M., C. Elicker, C. F. P. Nunes, A. V. Bairros, E. M. Becker, D. Müller, D. Oliveira, E. Piva, L. A. M. Fontoura, and C. M. P. Pereira. 2016. "The Synthesis and Characterization of Butia Capitata Seed Oil as a FAME Feedstock." *Fuel* 184:96160. https://doi.org/10.1016/j.fuel.2016.07.052.

Wang, X., and P. Ni. 2017. "Combustion and Emission Characteristics of Diesel Engine Fueled with Diesel-Like Fuel from Waste Lubrication Oil, Energy Convers." *Energy Conversion and Management* 133:275–283. https://doi.org/10.1016/j.enconman.2016.12.018.

Wang, Y., S. Yang, G. Bao, and H. Wang. 2024a. "Pyrolysis of Macadamia Nut Peel Using Multicomponent Gaussian Kinetic Modeling and ANN Analysis." *Biomass and Bioenergy* 183:107170. https://doi.org/10.1016/j.biombioe.2024.107170.

Wang, Y., S. Yang, G. Bao, and H. Wang. 2024b. "Pyrolytic Characteristics of Abutilon Stalk Waste Using tg-Ftir, py-Gc/ms, and Artificial Neural Networks: Kinetics, Thermodynamics, and Gaseous Products Distribution." *Journal of Analytical and Applied Pyrolysis* 178:106403. https://doi.org/10.1016/j.jaap.2024.106403.

Xu, F., B. Wang, D. Yang, J. Hao, Y. Qiao, and Y. Tian. 2018. "Thermal Degradation of Typical Plastics Under High Heating Rate Conditions by tg-Ftir: Pyrolysis Behaviors and Kinetic Analysis." *Energy Convers managenergy Conversion and Management* 171:1106–1115. https://doi.org/10.1016/j.enconman.2018.06.047.

Yu, D., S. Hu, L. Wang, Q. Chen, and N. Dong. 2020. "Comparative Study on Pyrolysis Characteristics and Kinetics of Oleaginous Yeast and Algae." *International Journal of Hydrogen Energy* 45:10979–10990. https://doi.org/10.1016/j.ijhydene.2020.02.052.

Yunus, S., A. Abd, N. Rosli, and R. Mamat. 2013. "Emissions of Transesterification jatropha-Palm Blended Biodiesel." *Procedia Engineering* 68:265–270. https://doi.org/10.1016/j.proeng.2013.12.178.

Zikhali, V. N., C. Mpofu, D. Nyama, B. Nyoni, and K. Mushonga. 2023. "Kinetic and Thermodynamic Analysis of Chicken Manure Pyrolysis for Sustainable Waste Management in the Poultry Industry Kinetic and Thermodynamic Analysis of Chicken Manure Pyrolysis for Sustainable Waste Management in the Poultry Industry." *Scholars*

International Journal of Chemistry and Material Sciences 6 (6): 135–140. https://doi.org/10.36348/sijcms.2023.v06i06.003.

Zsinka, N. M. V. 2024. "b.Levente Tarcsay, Determination of Kinetic and Thermodynamic Parameters of Biomass Gasification with tg-Ftir and Regression Model Fitting." *Energie* 17 (8): 1875. https://doi.org/10.3390/en17081875.

Zuo, Z., Q. Yu, H. Xie, W. Duan, S. Liu, and Q. Qin. 2017. "Thermogravimetric Analysis of the Biomass Pyrolysis with Copper Slag as Heat Carrier Pyrolysis Characteristics and Kinetics." *Journal of Thermal Analysis and Calorimetry* 129 (2): 1233–1241. https://doi.org/10.1007/s10973-017-6174-y.